Seasonal and spatial variability in the optical characteristics of DOM in a temperate shelf sea

Nealy Carr[a,*], Clare E. Davis[a], Sabena Blackbird[a], Lucie R. Daniels[b], Calum Preece[a], Malcolm Woodward[c], Claire Mahaffey[a]

[a] Department of Earth, Ocean and Ecological Sciences, University of Liverpool, Liverpool, UK
[b] Ocean and Earth Science, University of Southampton, National Oceanography Centre Southampton, Southampton, UK
[c] Plymouth Marine Laboratory, Prospect Place, The Hoe, Plymouth, UK

ARTICLE INFO

ABSTRACT

The Celtic Sea is a productive temperate sea located on the Northwest European Shelf. It is an important pathway for the delivery of land-derived material to the North Atlantic Ocean, including dissolved organic matter (DOM). The aim of this study was to determine the seasonal and spatial variability in the magnitude, source and composition of DOM at three sites representing on shelf, central shelf and shelf edge regions in the Celtic Sea, using observations collected during the UK Shelf Sea Biogeochemistry (SSB) research programme (November 2014 – August 2015). The concentration of dissolved organic carbon (DOC) alongside DOM absorbance and fluorescence indices were measured and fluorescence Excitation and Emission Matrices (EEMs) combined with Parallel Factor Analysis (PARAFAC) were used to assess DOM composition and lability. The PARAFAC model identified four unique fluorescent components for autumn (November 2014), winter (March 2015), spring (April 2015) and summer (July 2015) consisting of two humic-like components attributed to terrestrial (C1) and marine sources (C2), and two protein components identified as tyrosine-like (C3) and tryptophan-like (C4) attributed to in situ production. DOC varied seasonally and there were strong cross shelf trends. The protein components (C3 and C4) exhibited large seasonal and within season variability particularly during productive periods. In contrast, there were persistent cross shelf gradients in the CDOM absorption coefficient at 305 nm (a305), the UV specific absorbance at 280 nm (SUVA$_{280}$), the humification index (HIX), and the humic-like fluorescent components (C1 and C2), which were higher in the on shelf region and decreased towards the shelf edge. The humic-like components and the slope ratio (SR) were significantly correlated with salinity throughout all seasons, indicating a strong influence of terrestrially-derived organic matter in the Celtic Sea, with potentially up to 35% of DOC in the central shelf during winter originating from terrestrial inputs. Results from this study illustrate the importance of monitoring DOM quantitatively and qualitatively for a better understanding of the supply, production, cycling and export of this dynamic organic carbon pool in shelf seas.

1. Introduction

Dissolved organic matter (DOM) is the largest pool of organic material in the ocean, storing up to fifty times more carbon (C) than that stored in the particulate pool (POC $18 \pm 5 \times 10^{15}$ g C (Eglinton and Repeta, 2006). The amount of dissolved organic carbon (DOC) in the ocean (685×10^{15} g C) is comparable to the amount of carbon as CO_2 in the atmosphere (Hansell and Carlson, 1998, Hansell et al., 2009)).

DOM is produced autochthonously by plankton in the surface ocean during primary and secondary production (Hansell and Carlson, 2001, Hansell et al., 2009), with substantial amounts being released or exuded by phytoplankton (Hygum et al., 1997, Jiao et al., 2010).

Mesozooplankton mediate the release of DOM and up to 50% of suspension filtered food can be released as DOM during grazing activity (Hygum et al., 1997). Viral cell lysis (Suttle, 2005, Suttle, 2007) and bacteria (Jiao et al., 2010) cause DOM release from particulate organic matter (POM). Rivers are also an important source of externally supplied DOM from terrestrial origin to the marine environment. Syntheses of past and recent global estimates show that rivers, as part of the land-ocean continuum, contribute around 0.25×10^{15} g C yr^{-1} to the global ocean as DOC (Hedges et al., 1997, Cai, 2011, Raymond and Spencer, 2015).

In the upper 100 m of the open ocean, DOC concentrations vary from 34 to 80 μM (Sipler and Bronk, 2015). DOC concentrations are

---

higher in coastal and continental shelf regions, reaching up to 140 µM in coastal waters at a salinity greater than 35 (Barron and Duarte, 2015). The strong inverse relationship between salinity and DOC in estuarine and coastal environments (Barron and Duarte, 2015), continental shelf seas (Mendoza and Zika, 2014) and the open ocean (Kowalczuk et al., 2013) highlights the importance of land as a source of DOC in the marine environment. Employing the empirical relationship reported in Barron and Duarte (2015), 9 µM of DOC is lost when salinity increases by 1 unit.

Heterotrophic utilisation and remineralisation is the largest biotic sink of DOC in the aerobic ocean (Hansell et al., 2009). As the most abundant microorganisms in the surface ocean, bacterioplankton help shunt DOM towards the microbial loop where it is remineralised to its inorganic constituents i.e. dissolved inorganic carbon (DIC), DIN and DIP (Hansell and Carlson, 2015).

Knowledge of the composition of DOC is important for understanding how DOC is cycled in the water column and identifying the sources and sinks (Hansell and Carlson, 2015). However, determining the source, composition and lability of DOC is not straightforward, and requires analytically complex geochemical techniques, for example, to distinguish between high molecular weight compounds and humic substances (Aluwihare et al., 2002, Repeta et al., 2002), or to unravel DOM molecular complexity (Stubbins et al., 2014). A simple approach is to use vertical distributions to infer bulk properties of DOM. In the open ocean, DOC at 1000 m is considered to be refractory and can thus be subtracted from surface ocean DOC concentrations to reveal the partitioning of DOC into labile, semi-labile, semi-refractory, refractory and ultra-refractory pools (Hansell, 2013, Hansell and Carlson, 2015). However, in the shelf seas, this simple view does not work due to (a) the vertical exchange between the shallow surface mixed layer (SML) and bottom mixed layer (BML) by tides and turbulent mixing which smears out vertical gradients in DOM (b) multiple sources of DOM, for example, from freshwater inputs and sediments and (c) strong productivity events (spring and autumn blooms) or interactions (grazing pressure) that consume or release DOM. Thus, alternative approaches must be used to better understand the dynamics of DOM in shelf seas, as well as its source and lability.

A number of studies (Hopkinson and Vallino, 2005, Barron and Duarte, 2015) highlight the importance of DOM in biogeochemical nutrient cycling and DOC on global carbon export. However, DOM production and composition in shelf seas and the subsequent export of carbon at continental margins is less well understood (Liu et al., 2010). This study extends the application of EEM and PARAFAC modelling, a technique commonly employed across a wide range of aquatic and marine environments (Stedmon et al., 2003, Yamashita and Tanoue, 2003, Yamashita et al., 2011) to the seasonally stratified, temperate Celtic Sea region in the Northwest European Shelf. Here, for the first time, we use a combination of measurements on DOC concentrations alongside DOM absorbance and fluorescence EEMs coupled with PARAFAC modelling to assess the source and lability of DOM on seasonal time scales at three physically distinct sites in the Celtic Sea. Our goal was to assess the contribution of land-derived DOC to the DOM pool in the Celtic Sea and to determine how lability was affected by productivity events in the Celtic Sea.

2. Materials and methods

2.1. Sampling

As part of a Natural Environment Research Council (NERC) funded SSB programme, cruises were conducted between November 2014 and August 2015 on the Northwest European Shelf region and in the North Atlantic (Fig. 1), aboard the *RRS Discovery*. Seawater samples were collected during four cruises, November 2014, March 2015, April 2015 and July 2015, representing autumn, winter, spring and summer respectively. Samples were collected from three stations representing on

shelf (Site A), the Central Celtic Sea (CCS) and shelf edge regions. Seawater samples were collected at discrete depths ranging from 3 to 242 m using Niskin bottles attached to a rosette frame with a sensor package consisting of a Sea-Bird conductivity-temperature-depth (CTD) sensors and fluorometer. Sensors were calibrated using discrete samples collected during each cruise and fluorescence was calibrated to chlorophyll *a* mg m^{-3} by analysis of extracted samples filtered through Whatman glass fibre filters (GF/F, nominal pore size 0.7 µm) as described in (Mayers et al., this issue). The determination of dissolved inorganic nutrients are described in (Humphreys et al., this issue). The depth of the base of the thermocline was defined as the depth at which temperature deviated by > 0.05 °C from the lowest temperature. Below the base of the thermocline was defined as the bottom mixed layer (BML) and above the base of the thermocline was defined as the surface mixed layer (SML).

2.2. DOC and DOM fluorescence and absorbance

Samples for measurement of DOC were collected by filtering seawater through a combusted glass fibre filter (GF/F) under low vacuum pressure (< 10 mm Hg). Samples were preserved with 20 µL of 50% (v/v) hydrochloric acid and analysed onshore using high temperature catalytic oxidation (HTCO) on a Shimadzu TOC-V$_{CPN}$. The limits of detection for DOC were 3.4 µM with a precision of 2.5%. Consensus Reference Materials from the Hansell laboratory, Miami were analysed daily with a mean and standard deviation for DOC of 43.9 ± 1.2 µM (expected range 42–45 µM; n = 39). DOM samples collected for fluorescence and absorbance measurements were immediately filtered through a GF/F as above. In addition, samples were filtered through 0.2 µm polycarbonate filters under low vacuum pressure (< 10 mmHg), and stored in the dark at 5 °C until on-board analysis within five days of collection.

2.3. Fluorescence and absorbance

2.3.1. Excitation emission matrices (EEMs)

Water samples were brought to room temperature and fluorescence measurements were obtained using a spectrofluorometer (Horiba FluoroMax-4). Scan settings were configured for emission from 290 to 600 nm at 2 nm increments, excitation between 250 and 450 nm at 5 nm increments and band width set to 5 nm for both excitation and emission monochromators. Fluorescence spectra were acquired in instrument corrected mode (S1c/R1c) at 0.25 s integration time. EEMs were corrected by subtraction with Milli-Q water blank analysed daily, and for inner filter effects using sample absorption spectra measured using a UV–Vis spectrophotometer (Shimadzu 1650PC). EEMs were calibrated against the area under the water Raman peak (excitation at 350 nm) from Raman scans analysed daily and the resultant spectra are in Raman Units (R.U.). EEM corrections and calibrations were carried out using the drEEM (0.2.0) MATLAB toolbox (Murphy et al., 2013).

2.3.2. PARAFAC modelling

The three way EEM spectra of DOM fluorescence are modelled using a multi-way data analysis that decomposes the data matrix into a set of trilinear terms and a residual array (Eq. (1), The PARAFAC Model). The model was fitted to minimise the sum of squared residuals (Andersson and Bro, 2000, Stedmon et al., 2003).

$$x_{ijk} = \sum_{f=1}^{F} a_{if}\, b_{jf}\, c_{kf} + e_{ijk}, \quad i = 1,...,I;\ j = 1,...,J;\ k = 1,...,K. \tag{1}$$

For analysis of EEM spectra, χ_{ijk} is the fluorescence intensity for the *i*th sample at emission wavelength *j* and excitations wavelength *k*. The *f* corresponds to individual PARAFAC components and each component has *a*-values (scores) for each sample, *b*-values (emission loadings) for each emission wavelength and *c*-values (excitation loadings) for each
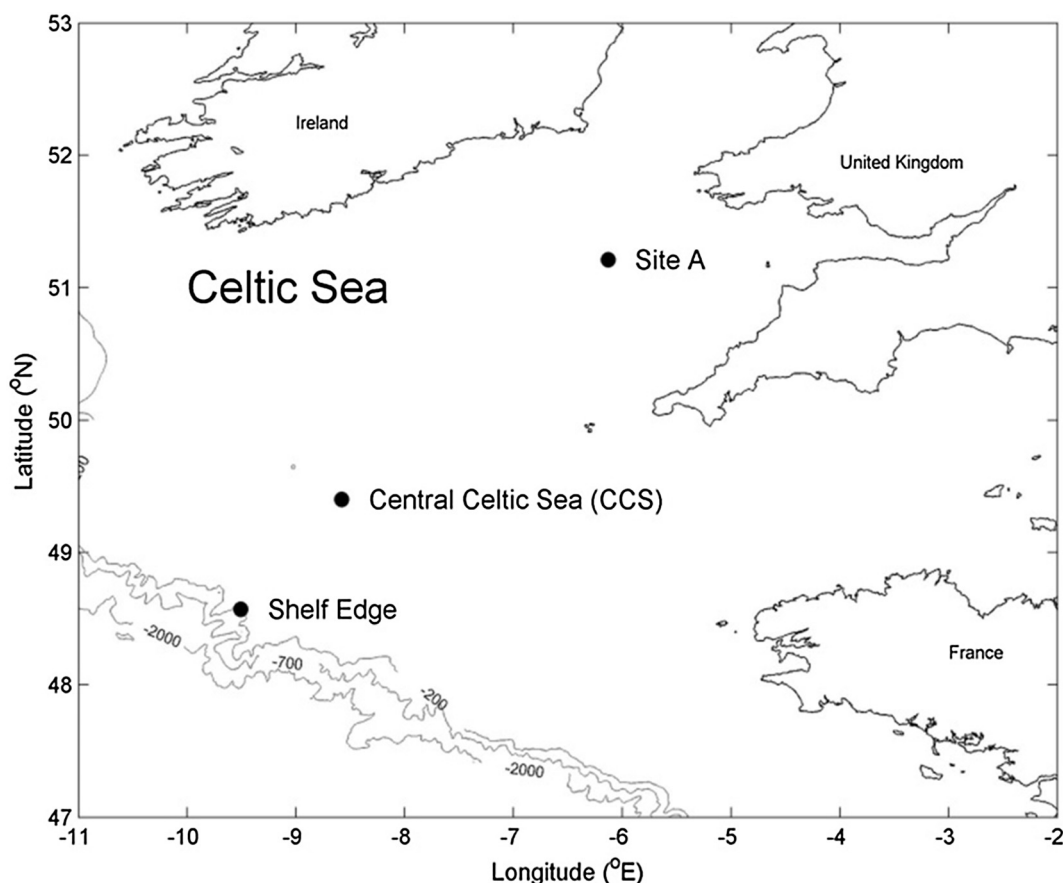
Fig. 1. Map showing the location of the shelf edge, central shelf (CCS) and on shelf (Site A) stations sampled during SSB research cruises.

excitation wavelength, where *b* and *c* are scales estimates of emission and excitation spectra at wavelengths *j* and *k* respectively. Variability within the EEM spectra not captured by the model is contained in the data array e_{ijk}. For a detailed description of employing PARAFAC modelling, principles and approaches, and applying equation 1 to three way data arrays see (Bro, 1997, Stedmon and Bro, 2008, Murphy et al., 2013).

The fluorescent components of the corrected and calibrated EEM spectra were modelled using Parallel Factor Analysis (PARAFAC) following the methods as described by (Murphy et al., 2013). The PARAFAC modelling was carried out using MATLAB 8.3.0.532 (R2014a) with the DOMFluor toolbox and data sets from each cruise were inserted into the model separately. EEMs were corrected and calibrated using the drEEM (0.2.0) MATLAB toolbox (Murphy et al., 2013). To reduce random noise introduced from lower wavelengths and secondary Raman and Rayleigh scatter, PARAFAC models were applied to a reduced EEM range of 270–450 nm and 290–500 nm for excitation and emission wavelengths respectively. Each data array consisted of between 106 and 198 samples with 37 excitation and 106 emission wavelengths. For each dataset, models were initially fit using between two and six components, and the number of components were selected when a reasonble fit above 97% was obtained. To ensure a least squares and global solution, the estimated fluorescent DOM components identified in each dataset were validated using random initialisation and split half analysis (Stedmon and Bro, 2008).

2.3.3. DOM fluorescent component assignment

3D fluorescense and the resolved excitation and emission spectral loadings of the components identified by the PARAFAC model are shown in Fig. 2, while Table 1 summarises spectral characteristics with references to comparitive components identified globally from coastal,

shelf sea and oceanic environments. Components were assigned to terrestrial UVC humic material of allochthonous orign (C1), UVA humic-like of both terrestrial and marine origin (C2), and two protein-like components tyrosine (C3) and tryptophan (C4) of biological autochthonous origin. The DOM pool is a complex mixture of organic molecules in which a fraction absorbs light (CDOM) and a sub fraction of this absorbing pool emits light as fluorescence (FDOM). Assigning source and lability based on DOM fluorescence alone is challenging as an increasing number of studies have indicated that humic-like fluorescence can result from diagenesis of DOM regardless of source i.e. autochthonous and allochthonous (Lu et al., 2015), as well as production from microalgae (Jorgensen et al., 2011, Bai et al., 2017) and picocyanobacteria produced humic-like fluorescence found in the deep ocean (Zhao et al., 2017). The characterisations assigned to PARAFAC modelled DOM components identified in this study are based on their spectral characteristics and on published comparable studies of component fluorescence spectra, behaviour and distribution, across the freshwater-marine continuum including but not limited to (Kowalczuk et al., 2013, Mendoza and Zika, 2014, Pitta et al., 2016).

2.3.4. Spectral indices

Water samples were allowed to reach room temperature and absorbance measurements were obtained using a UV–Vis spectrophotometer (Shimadzu 1650PC). The instrument baseline correction was performed before sample analysis. Chromophoric dissolved organic matter (CDOM) absorbance was measured from 250 to 800 nm at 1 nm increments (2 nm, slit width) with Milli-Q water as the reference blank. Raw absorbance was corrected for instrument drift, temperature effects, scattering and refractive effects by subtracting the average absorbance between 700 and 800 nm from the absorbance spectrum (Green and Blough, 1994, D'Sa et al., 1999, Helms et al., 2008). Absorption
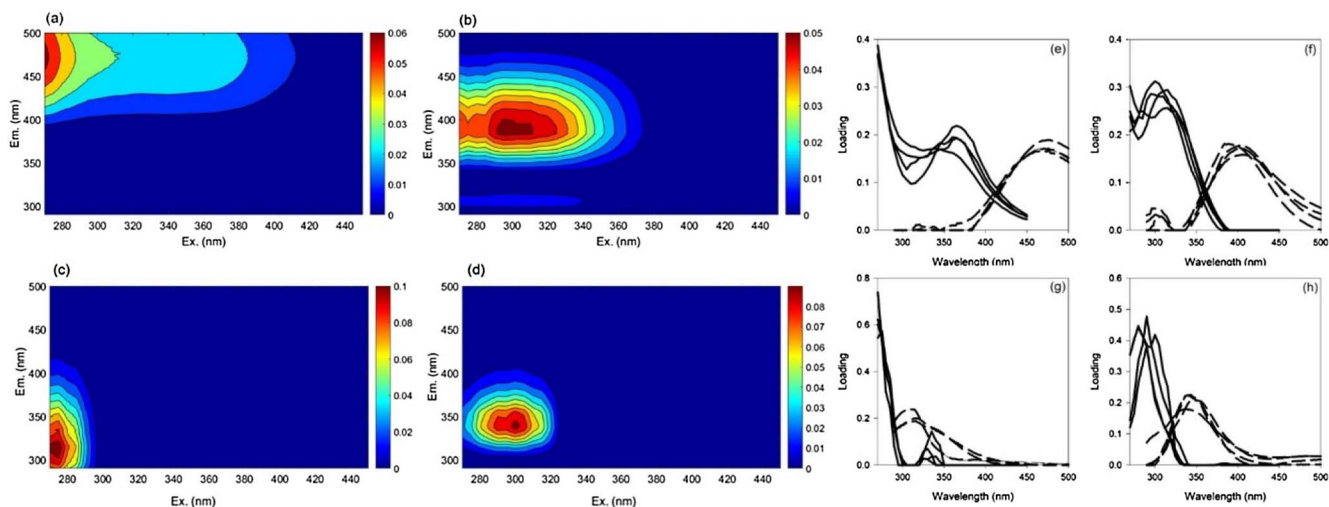
N. Carr et al.

Fig. 2. The PARAFAC model output for the winter dataset showing the fluorescence signatures of four components identified, C1 (a), C2 (b), C3 (c) and C4 (d). Spectral loadings for each component for all datasets (excitation spectra solid black line and emissions spectra dotted black line), C1 (e), C2 (f), C3 (g) and C4 (h).

coefficients were obtained from absorbance spectrum as follows:

$$a = 2.303A/l, \qquad (2)$$

where a is the absorption coefficient in m^{-1} at a reference wavelength, A is the raw absorbance at the reference wavelength and l is the path length of the cell in metres. As a measure of CDOM concentrations, the absorption coefficient at 305 was chosen for comparison with results from previous work in the Celtic sea region (Kowalczuk et al., 2013). The spectral slope coefficient of CDOM, S, is a descriptor of CDOM absorbance spectra and is inversely proportional to molecular weight, and used to characterise DOM composition (Stedmon and Nelson, 2015). For this study, S was calculated between 300 and 650 nm using a non-linear regression technique according to (Stedmon et al., 2000). This range was chosen as it is within the wavelength range that captures changes in CDOM composition due to production and photochemical alterations (Nelson and Siegel, 2013), and it is relevant to remote sensing applications (Stedmon et al., 2011). The spectral slope ratio (SR) of the absorbance spectra is used as an indicator of the molecular weight (MW), source and photobleaching of CDOM (Helms et al., 2008). For this study, the slope coefficient values for slopes between 275 and 295 nm, and between 350 and 400 nm were obtained from linear regression of log transformed absorbance spectra using MATLAB

8.3.0.532 (R2014a). The SR was then calculated as the ratio between the two slopes. Low SR values are generally attributed to higher MW DOM of terrestrial origin e.g. ~0.7 for terrestrial and ~1.1 for estuarine and coastal samples, while increases in SR values can be photochemically induced and decreases due to microbial processing (Helms et al., 2008). The specific ultraviolet absorbance (SUVA) is calculated by normalising decadic absorption to DOC concentrations and has been shown to be is positively correlated with molecular weight and an indicator of aromaticity of aquatic humic substances (Weishaar et al., 2003). Here SUVA was calculated at 280 nm ($SUVA_{280}$). The humification index (HIX) was calculated according to (Zsolnay et al., 1999) as the ratio of emission 434–480 nm to the peak emission area 300–346 nm at 254 nm excitation. The HIX is an indicator of humic substances and extent of humification of organic matter (Hansen et al., 2016). High HIX is characterised by high molecular weight humic acids (Zsolnay et al., 1999, Kowalczuk et al., 2013) and higher values indicate greater humification of the source material (Ohno, 2002). The fluorescence index (FI) was calculated according to (McKnight et al., 2001) as the ratio of emission at 450 nm to emission at 500 nm at 370 nm excitation. The FI is used to differentiate between microbially derived fulvic acids, index value ~1.9, and terrestrially derived fulvic acids, index value ~1.4 (McKnight et al., 2001). The biological index

Table 1
Peak description of PARAFAC modelled DOM fluorescent components and their source assignment for this study.

Component	Peak max position Ex/Em	Coble peak[a]	Source assignment
C1	270/470–478	A	UVA humic-like, terrestrial, allochthonous Component 3: 270 (360)/478 (Stedmon et al., 2003) Component 1: < 250 (320)/422 (Yamashita et al., 2011) Component 2: 240 (370)/480 (Kowalczuk et al., 2013)
C2	295–315/384–406	M	UVC marine humic-like, terrestrial, microbial Component 4: < 250 (295)/358 (Yamashita et al., 2011) Component 5: 300/408 (Kowalczuk et al., 2013) Component 2(HLC2): 250(310)/410 (Mendoza and Zika, 2014) Component 2: 300/402 (Pitta et al., 2016)
C3	270–275/310–314	B	Tyrosine-like, protein-like, autochthonous, biological, microbial Component 4: 300/408 (Kowalczuk et al., 2013) Component 5(TLC5): 270/305 (Mendoza and Zika, 2014) Component OP6: 275/308 (Yamashita et al., 2015)
C4	280–300/338–344	T	Tryptophan-like, protein-like, autochthonous, biological, microbial Component 6: 280/328 (Murphy et al., 2008) Component 5: 280/334 (Yamashita et al., 2011) Component 6: 295/334(360) (Kowalczuk et al., 2013)

[a] Coble (1996).

(BIX) was calculated according to (Huguet et al., 2009) as the ratio of emission at 380 nm to emission at 430 nm at 310 nm excitation. The BIX is an indicator of freshly produced autochthonous DOM, with higher values indicating a higher proportion of fresh DOM (Huguet et al., 2009, Hansen et al., 2016).

2.4. Statistical analysis, correlations and linear regressions

Statistical analysis was performed using SigmaPlot version 13.0, Systat Software, Inc. SigmaPlot for Windows. Paired t-tests were used to determine significant differences for groups of data between sites and seasons, and the Mann-Whitney Rank Sum Test was used when data was not normally distributed. Differences were deemed statistically significant when the p value was < 0.05. Linear regression analysis was used to identify significant correlations between parameters and correlations deemed significant when p values of regression coefficients were < 0.05.

3. Results

3.1. Seasonal and spatial variation in hydrography, chlorophyll a and inorganic nutrients

The seasonal and vertical variation in salinity, temperature and chlorophyll *a* (Fig. 3a–i) and nitrite plus nitrate (N + N) (Fig. 4a–c) for the three stations sampled in the Celtic Sea highlight the seasonality observed at each site.

At Site A, surface waters were cooler and fresher in winter and spring than in autumn, and remained fresher with increasing temperatures in summer (Fig. 3c and f, and Table 2). Surface salinity varied seasonally by 0.5. Temperature gradients between the SML and BML in autumn (0.87 °C), winter (0 °C) and spring (1.04 °C) were small indicating either a completely mixed or weakly stratified water column. In contrast, the SML-BML temperature difference was 5.61 °C in summer, indicating a stratified water column. Mean surface chlorophyll *a* concentrations were highest in spring and autumn, respectively, indicative of bloom events, and were low in summer and winter (Fig. 3i and Table 2). Subsurface chlorophyll maxima (SCM) were evident in summer, with concentrations reaching 1 mg m^{-3} within the SCM compared to 0.44 mg m^{-3} at the surface. There were strong vertical gradients in nitrate between the SML and BML in autumn (6 μM), spring (7.4 μM) and summer (9.5 μM) but gradients were weak in winter (0.11 μM, Fig. 4c).

At CCS, surface waters were cooler and fresher in winter and spring than in autumn, with higher temperature and salinity in summer (Fig. 3b and e, and Table 2). The water column was stratified in autumn and mixed in winter. Surface salinity varied seasonally by 0.1. The onset of stratification occurred in spring when the difference in temperature between the SML and BML ranged between 0.52 °C and 1.29 °C, compared to 5.91 °C in summer when the water column was strongly stratified. Mean surface chlorophyll *a* concentrations were highest in spring and autumn, respectively, indicating seasonal bloom events, and were low in summer and winter (Fig. 3h and Table 2). SCM were evident in the summer, with concentrations reaching 0.73 mg m^{-3} at the peak of the SCM. Again, there were strong vertical gradients in nitrate between the SML and BML in autumn (8 μM), spring (5.5 μM) and summer (8.5 μM) but gradients were weak in winter (0.14 μM) and early spring (1.1 μM, Fig. 4b).

At the shelf edge site, surface waters were cooler in winter and spring than in autumn, with increased temperature in summer (Fig. 3a and d, and Table 2). Surface salinity varied seasonally by 0.05. The water column was mixed in winter and stratified in autumn, with weak stratification in spring. In summer, the water column was strongly stratified, with the difference between SML and BML temperatures reaching 4.34 °C, compared to 1.87 °C in autumn and < 1 °C in spring. Surface chlorophyll *a* concentrations were highest in spring at

1.28 mg m^{-3} (mean 0.75 ± 0.46 mg m^{-3}) and summer 0.86 mg m^{-3}, and lowest in winter at 0.38 mg m^{-3} (Fig. 3g and Table 2). SCM were not observed at the shelf edge in summer. Again, there were strong vertical gradients in nitrate between the SML and BML in autumn (6 μM) and summer (9.4 μM) but gradients were weak in winter (0.1 μM) and spring (0.9 μM, Fig. 4a).

Surface waters were consistently cooler and fresher at Site A compared to CCS and the shelf edge throughout all seasons (Table 2). Cross shelf surface temperature gradients were strongest during winter (by 2.04 °C) and weakest in summer (by 0.71 °C). Conversely, the cross shelf gradient in surface salinity was most pronounced during summer (0.82) and weakest during autumn (0.36). Surface chlorophyll *a* concentrations were highest at Site A in spring (0.96 mg m^{-3}), at CCS in autumn and during the spring bloom (1.09 mg m^{-3} and 1.86 mg m^{-3}, respectively) and at the shelf edge in summer (0.86 mg m^{-3}). Surface chlorophyll *a* concentrations were lowest at Site A in winter (0.37 mg m^{-3}), at CCS in summer (0.14 mg m^{-3}) and at the shelf edge in autumn and spring (0.59 mg m^{-3} and 0.36 mg m^{-3}, respectively). There was a strong cross shelf gradient in N + N in the BML, with the highest concentrations (> 10 μM) and lowest concentrations (6.4 μM) at CCS (Fig. 4b).

3.2. Seasonal and spatial variation in DOC and PARAFAC modelled DOM components

Vertical gradients in DOC were weak except at Site A during autumn and the shelf edge during summer (Fig. 4f and d). The spatial and seasonal gradients in DOC were stronger than the vertical gradients and thus, to compare between sites and seasons, DOC measurements were integrated and depth-averaged (Fig. 5 and Table 2). The statistical significance of seasonal and spatial patterns are reported in Supplementary Tables 1 and 2.

At Site A, DOC was highest in autumn (84 μM ± 0.7 μM) and lowest in summer (63 μM ± 1.1 μM) (Fig. 5, Table 2, and Supplementary Table 1). At CCS, DOC concentrations were highest in spring (69 μM ± 1.3 μM) and lowest in summer (63 μM ± 1.1 μM) (Fig. 5, Table 2, and Supplementary Table 1). At the shelf edge DOC concentrations were highest in summer (73 μM ± 1.1 μM) and lowest in winter (64 μM ± 1.1 μM) (Fig. 5, Table 2, and Supplementary Table 1). There were strong seasonal cross shelf gradients in DOC, with DOC being higher at Site A and declining towards the shelf edge in autumn (by 19%, p > 0.05) and winter (by 21%, p < 0.05). In contrast, DOC was higher at the shelf edge and declined towards Site A in spring (by 3%, p > 0.05) and summer (by 14%, p < 0.05).

As with DOC, vertical gradients in DOM components were weak. Fluorescence intensity of the humic-like components, C1 (Fig. 4 g, h and i) and C2, was generally lower in the surface at all sites and increased with depth. For example, C1 increased with depth by 41% at Site A during spring, indicative of photodegradation in surface waters. The protein-like components varied with depth similarly to DOC, and were generally higher in the surface than at depth. Overall, components displayed profiles typical to those found in global trends (Jorgensen et al., 2011). However, seasonal variability (Fig. 6) and cross shelf gradients were more pronounced (Table 2) therefore water column measurements of fluorescence intensity were averaged for comparisons between seasons and sites.

At Site A, CCS and the shelf edge, C1 was highest in winter and lowest in summer, except at the shelf edge, when C1 was lowest in autumn (Fig. 6a–c, Table 2 and Supplementary Table 1). There were no consistent clear seasonal trends at each site for C2, the marine humics component. At Site A, C2 was highest in spring and summer and lowest in autumn but differences were not significant (Fig. 6a and b, Table 2 and Supplementary Table 1). At CCS, C2 was highest in spring and lowest in summer but at the shelf edge, C2 was highest in autumn and lowest in spring (Fig. 6b and c, Table 2 and Supplementary Table 1).

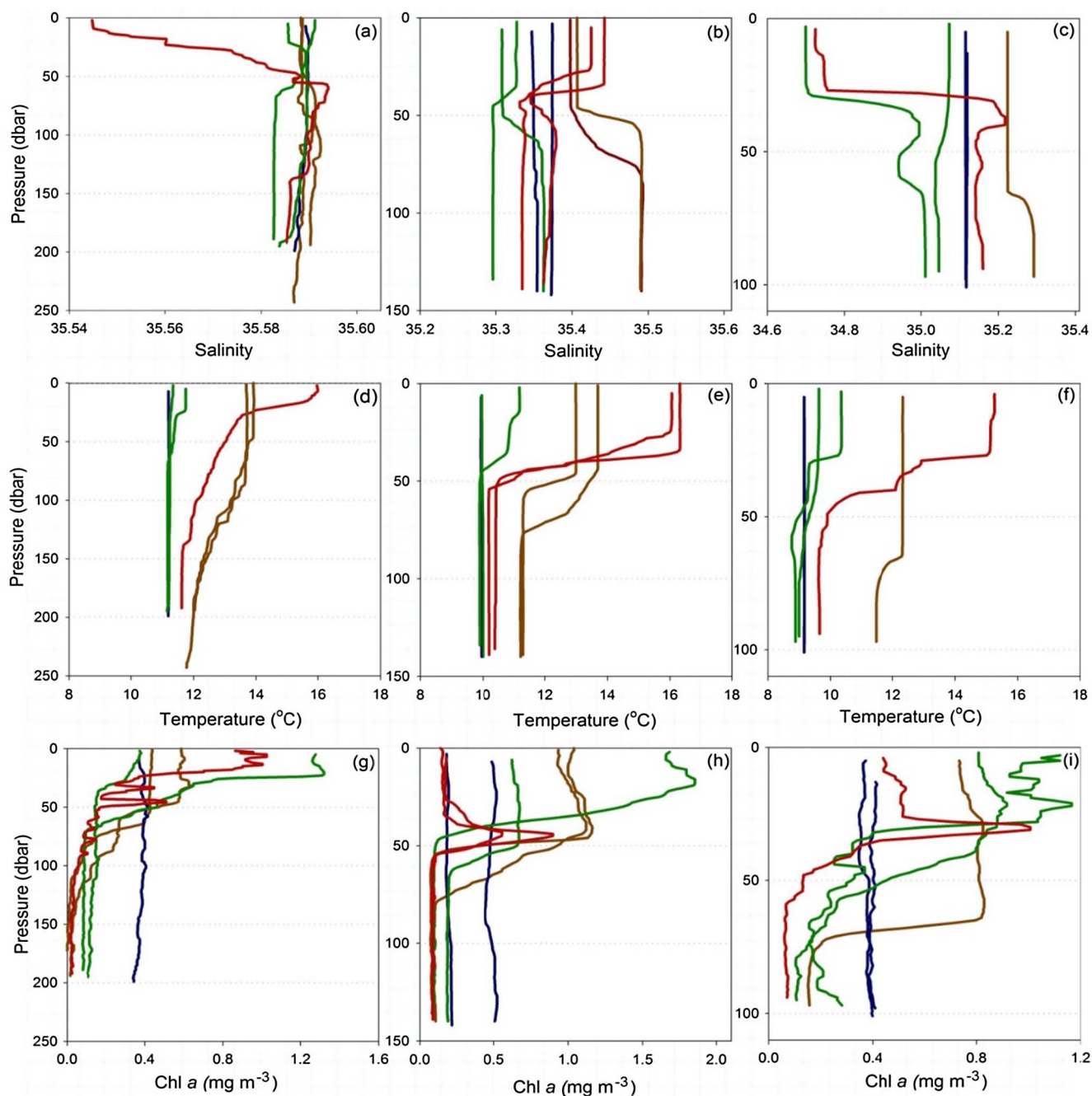C1 and C2 were at least twofold higher at Site A compared to the

Fig. 3. Vertical profiles of; salinity at (a) Shelf edge, (b) CCS and (c) Site A; temperature at (d) Shelf edge, (e) CCS and (f) Site A; and chlorophyll *a* fluorescence at (g) Shelf edge, (h) CCS and (i) Site A, for autumn (brown line), winter (blue line), spring (green line) and summer (red line), for CTD cast on initial and final visit (where applicable).

shelf edge during all seasons, resulting in a strong and significant cross shelf seasonal gradient in humic material (Table 2 and Supplementary Table 2). The dominance of C1 at Site A indicates the impact of terrestrial organic matter in this region and suggests that the distribution is the result of seasonal variability in the supply and transport and dilution of this component.

There was greater variability in the seasonal rather than cross shelf trends in C3 and C4, the two protein-like components. Overall fluorescence intensity of these components were up to four times greater than the humic-like components (Fig. 6). At Site A, there were no significant seasonal trends in C3, the tyrosine-like amino acid component. However, C3 increased from $0.020 \, \text{R.U.} \, \text{nm}^{-1}$ to $0.031 \, \text{R.U.} \, \text{nm}^{-1}$ at Site A between visits two days apart during winter. This increase was coincident with a 12% increase in surface chlorophyll *a* concentrations (from $0.37 \, \text{mg} \, \text{m}^{-3}$ to $0.41 \, \text{mg} \, \text{m}^{-3}$) and a 21% increase in surface DOC

(from 73 µM to 94 µM) at this site over the same period.

At CCS, C3 was highest in winter and more than double that of the lowest values in autumn (Fig. 6b, Table 2 and Supplementary Table 1). During the development of the spring bloom, C3 more than doubled from $0.015 \pm 0.003 \, \text{R.U.} \, \text{nm}^{-1}$ to $0.041 \pm 0.012 \, \text{R.U.} \, \text{nm}^{-1}$, and was coincident with a threefold increase in surface chlorophyll *a* concentrations ($0.62 \, \text{mg} \, \text{m}^{-3}$ to $1.68 \, \text{mg} \, \text{m}^{-3}$). Conversely, C3 decreased by 50% ($0.035 \pm 0.006 \, \text{R.U.} \, \text{nm}^{-1}$ to $0.018 \pm 0.008 \, \text{R.U.} \, \text{nm}^{-1}$) over a two-week period during summer as surface chlorophyll *a* concentrations decreased by 22% ($0.18–0.14 \, \text{mg} \, \text{m}^{-3}$).

At the shelf edge, C3 was highest in spring, more than treble that of the lowest values in summer (Fig. 6c, Table 2 and Supplementary Table 1). In spring, C3 increased by threefold over a five hour period ($0.014 \pm 0.003 \, \text{R.U.} \, \text{nm}^{-1}$ to $0.048 \pm 0.009 \, \text{R.U.} \, \text{nm}^{-1}$), and more than doubled within a week during the spring bloom period (to
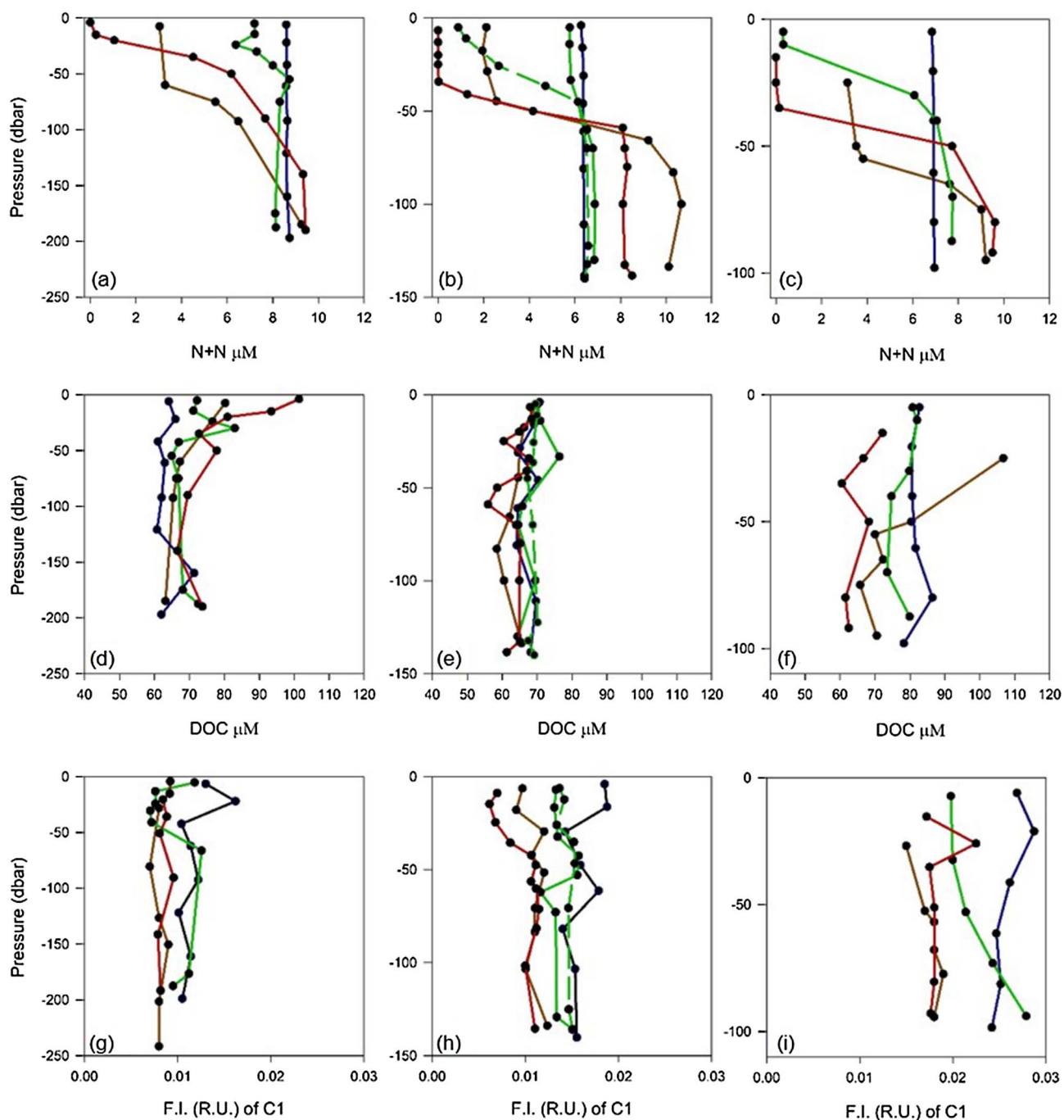
N. Carr et al.

Fig. 4. Vertical profiles of averaged; inorganic nutrients (N + N) at Shelf edge (a), CCS (b) and Site A (c); DOC at Shelf edge (d), CCS (e) and Site A (f); and PARAFAC model component C1 at Shelf edge (g), CCS (h) and Site A (i), for autumn (brown line), winter (blue line), spring (green line) and summer (red line). (For interpretation of the references to colour in this figure legend, the reader is referred to the web version of this article.)

0.037 ± 0.012 R.U. nm^{-1}), when surface chlorophyll a concentrations increased nearly threefold (0.36–0.99 mg m^{-3}).

At Site A, C4, the tryptophan-like amino acid component, was highest in summer and twice that of the lowest values in winter (Fig. 6a, Table 2 and Supplementary Table 1). At CCS, C4 was highest in spring and twice that of the lowest values in autumn (Fig. 6b, Table 2 and Supplementary Table 1). Similarly to C3, C4 more than doubled over a three-week period during the development of the spring bloom (0.011 $\pm$ 0.002 R.U. nm^{-1} to 0.028 $\pm$ 0.007 R.U. nm^{-1}), and decreased by 25% between visits one day apart in summer. At the shelf edge differences in C4 were only significant between autumn and

summer (Fig. 6c, Table 2 and Supplementary Table 1). Similarly to C3, there were significant differences during the development of the spring bloom when C4 increased by over threefold (0.006 $\pm$ 0.000 R.U. nm^{-1} to 0.022 $\pm$ 0.006 R.U. nm^{-1}) within a week. And, coincident with C3, C4 increased fivefold between visits only five hours apart (0.006 $\pm$ 0.000 R.U. nm^{-1} to 0.030 R.U. nm^{-1}).

Cross shelf gradients in C3 and C4 were not as clear compared with C1 and C2, and the direction of the gradient changed with each season. However, the gradient in C3 was only significant in winter and summer, when C3 was higher at CCS than at the shelf edge by 39% and 60%, respectively (Fig. 6b and c, and Supplementary Table 2). The cross shelf

Table 2

Average surface temperature, salinity and chlorophyll *a* concentrations, integrated and depth averaged DOC, and average water column fluorescence intensity of PARFAC modelled components (C1–C4) (± symbols are one standard deviation of the average, thus representing the water column fluorescence variability within seasons). Table indicates sample size for which averages were calculated.

Parameter	Season	Site A	Sample size	Central Celtic Sea (CCS)	Sample size	Shelf Edge	Sample size
Surface temperature (°C)	Autumn	12.33		13.41		13.91	
	Winter	9.16		10.01		11.2	
	Spring	9.98		10.34		11.5	
	Summer	15.26		16.28		15.97	
Surface salinity	Autumn	35.22		35.4		35.58	
	Winter	35.12		35.36		35.59	
	Spring	34.89		35.32		35.59	
	Summer	34.72		35.42		35.54	
Surface chlorophyll *a* (mg m^{-3})	Autumn	0.73		1.00		0.59	
	Winter	0.38		0.44		0.38	
	Spring	0.96		0.88		0.75	
	Summer	0.44		0.17		0.86	
DOC (µM)	Autumn	83.9 ± 0.7	6	65.7 ± 0.6	20	67.9 ± 0.9	10
	Winter	80.4 ± 0.9	12	65.2 ± 1.1	16	63.5 ± 1.1	8
	Spring	67.1 ± 1.3	12	68.5 ± 1.3	39	69.4 ± 1.3	14
	Summer	62.7 ± 1.1	6	63.4 ± 1.1	31	73.1 ± 1.1	8
C1 (R.U.)	Autumn	0.018 ± 0.001	6	0.011 ± 0.002	19	0.008 ± 0.001	6
	Winter	0.026 ± 0.002	12	0.016 ± 0.002	26	0.012 ± 0.002	8
	Spring	0.023 ± 0.003	7	0.014 ± 0.002	40	0.010 ± 0.003	18
	Summer	0.018 ± 0.002	6	0.010 ± 0.002	27	0.009 ± 0.001	8
C2 (R.U.)	Autumn	0.016 ± 0.001	6	0.011 ± 0.002	19	0.009 ± 0.000	6
	Winter	0.017 ± 0.001	12	0.011 ± 0.002	26	0.008 ± 0.001	8
	Spring	0.018 ± 0.002	7	0.012 ± 0.002	40	0.007 ± 0.002	18
	Summer	0.018 ± 0.002	6	0.010 ± 0.003	27	0.008 ± 0.001	8
C3 (R.U.)	Autumn	0.019 ± 0.005	6	0.016 ± 0.014	18	0.013 ± 0.005	6
	Winter	0.025 ± 0.009	12	0.033 ± 0.016	26	0.020 ± 0.007	8
	Spring	0.020 ± 0.010	6	0.029 ± 0.016	36	0.031 ± 0.019	15
	Summer	0.017 ± 0.007	6	0.025 ± 0.010	27	0.010 ± 0.010	8
C4 (R.U.)	Autumn	0.015 ± 0.003	6	0.011 ± 0.006	18	0.009 ± 0.003	6
	Winter	0.011 ± 0.002	12	0.019 ± 0.025	26	0.016 ± 0.014	8
	Spring	0.016 ± 0.006	6	0.021 ± 0.009	36	0.015 ± 0.012	17
	Summer	0.020 ± 0.004	6	0.017 ± 0.003	27	0.014 ± 0.003	8

gradient in C4 was only significant in autumn and summer, when C4 was significantly higher at Site A compared to the shelf edge by 30% and 40%, respectively (Fig. 6a and c, and Supplementary Table 2). Relative to C1 and C2, C3 dominated at CCS and the shelf edge during periods of high productivity, for example, during the spring bloom, and varied significantly with season, indicating that this protein-like DOM pool is an important autochthonous component of the DOM pool across the shelf.
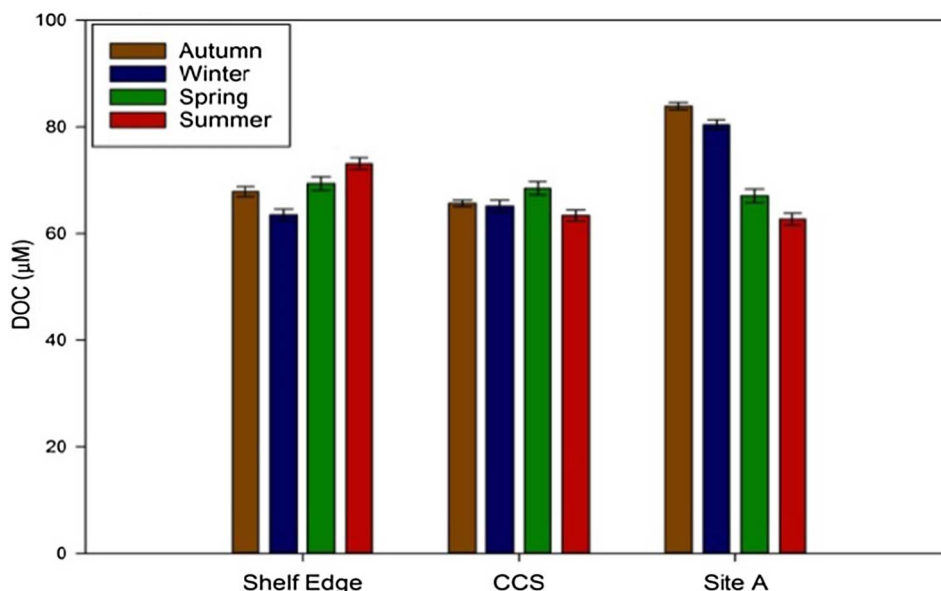

Fig. 5. Seasonal and cross shelf integrated and depth averaged DOC concentrations (µM). Error bars represent one standard deviation. Autumn (brown bar), winter (blue bar), spring (green bar) and summer (red bar). (For interpretation of the references to colour in this figure legend, the reader is referred to the web version of this article.)

Fig. 6. Seasonal and cross shelf distribution of fluorescence intensity in Raman Units (F.I. (R.U.)) of the PARAFAC modelled components, (a) C1, (b) C2, (c) C3, and (d) C4. Bar plots represent the average water column F.I. for all data. Whiskers are one standard deviation of the average, thus an indication of temporal and water column fluorescence variability. Autumn (brown bar), winter (blue bar), spring (green bar) and summer (red bar). (For interpretation of the references to colour in this figure legend, the reader is referred to the web version of this article.)
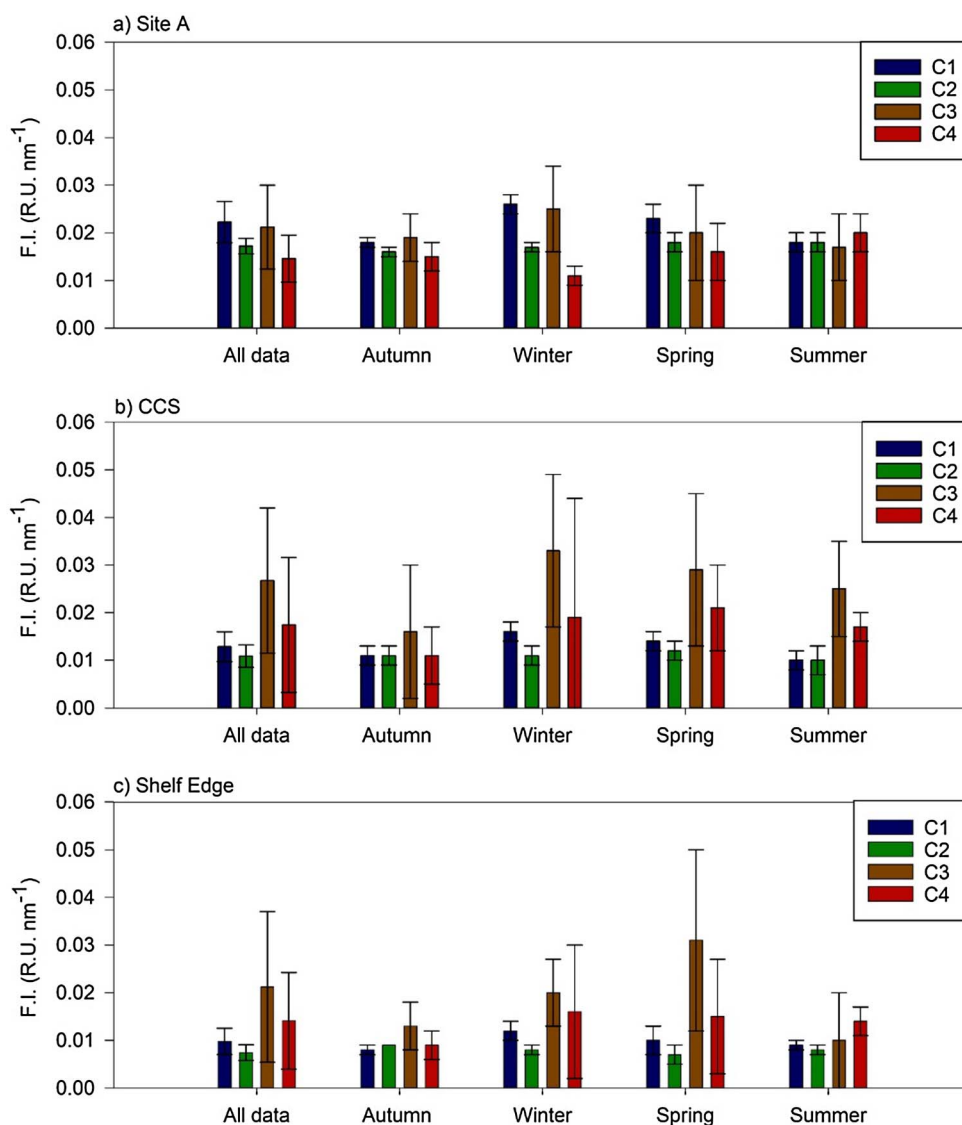
3.3. Seasonal and spatial variations in spectral and fluorescent indices

The spectral indices of absorption, the slope ratio (SR), absorption coefficient a305, slope coefficient $S_{300-650}$ and SUVA$_{280}$, and fluorescence indices, the humification index (HIX), fluorescence index (FI) and biological index (BIX) are summarised in Table 3. Except for a305, there were no strong vertical trends in either the spectral or fluorescence indices and thus indices were averaged over the entire water column. Note that absorbance data were not available for Site A in autumn.

For the entire data set, the SR ranged from 0.9 to 4.4 with seasonal means ranging from 1.8 ± 0.1 in summer to 3.1 ± 0.6 in autumn (Table 3). These SR values were within the range reported for shelf near-shore and offshore regions (1.7 and 4.6, respectively) (Helms et al., 2008, Kowalczuk et al., 2013, Catala et al., 2015). The lowest value of 0.9 was observed during winter and is indicative of influence of terrestrial DOM (Kowalczuk et al., 2013). Seasonality in the SR at Site A was not significant. At CCS and the shelf edge, the SR was highest in autumn and lowest in summer (Supplementary Table 1). Notably the SR increased at the shelf edge during the development of the spring bloom

by over 50% (from 2.2 ± 0.4 to 3.3 ± 0.5) (Fig. 7 insert bar chart). The CDOM absorption coefficient aCDOM(λ), here depicted as a305, ranged across the entire data set from 0.16 to 1.26 m^{-1}, with seasonal means ranging from 0.31 ± 0.10 in winter to 0.74 ± 0.08 in summer (Table 3). At Site A, a305 was highest in summer and lowest in winter (Supplementary Table 1). There were no clear seasonal trends in a305 at CCS and the shelf edge, but a305 was 23% higher in summer than winter at the shelf edge (Supplementary Table 1).

At Site A, variability in $S_{300-650}$ was low (range of 0.001 ± 0.002) and seasonal differences were not significant. At CCS and the shelf edge, $S_{300-650}$ was highest in autumn and lowest in summer (Table 3 and Supplementary Table 1).

At Site A and CCS, SUVA$_{280}$ was highest in summer compared to winter and autumn. Elevated SUVA$_{280}$ in summer coincided with low DOC and humic DOM suggesting that higher molecular weight material is produced in situ during the biodegradation of labile DOM produced during summer and the preceding spring. There were no significant seasonal patterns at the shelf edge.

The SR was higher at the shelf edge site compared to Site A (by 30–36%, p < 0.05, Fig. 7, Table 3), resulting in a strong cross shelf

Table 3

Water column averages of the SR, a305, $S_{300-650}$ and SUVA$_{280}$, HIX, FI and BIX values at three sites grouped according to season. ± symbols are one standard deviation of the average, thus representing the water column variability.

| Variable	Region	Autumn	Winter	Spring	Summer
Slope Ratio (SR)	Shelf Edge	3.1 ± 0.6	2.8 ± 0.7	3.0 ± 0.7	2.6 ± 0.4
	CCS	2.6 ± 0.6	2.4 ± 0.5	2.3 ± 0.4	2.2 ± 0.6
	Site A	No data	1.8 ± 0.2	1.9 ± 0.2	1.8 ± 0.1
$a305$ m^{-1}	Shelf Edge	0.39 ± 0.11	0.31 ± 0.10	0.45 ± 0.26	0.40 ± 0.05
	CCS	0.41 ± 0.10	0.43 ± 0.08	0.45 ± 0.15	0.44 ± 0.08
	Site A	No data	0.63 ± 0.05	0.68 ± 0.08	0.74 ± 0.08
$S_{300-650}$ (nm^{-1})	Shelf Edge	0.012 ± 0.002	0.016 ± 0.004	0.015 ± 0.006	0.016 ± 0.002
	CCS	0.011 ± 0.003	0.017 ± 0.003	0.015 ± 0.003	0.018 ± 0.004
	Site A	No data	0.018 ± 0.001	0.017 ± 0.002	0.017 ± 0.001
SUVA$_{280}$ (L mg C^{-1} m^{-1})	Shelf Edge	0.33 ± 0.08	0.42 ± 0.06	0.44 ± 0.14	0.41 ± 0.03
	CCS	0.41 ± 0.07	0.55 ± 0.09	0.48 ± 0.19	0.56 ± 0.11
	Site A	No data	0.56 ± 0.08	0.76 ± 0.30	0.79 ± 0.06
Humification Index (HIX)	Shelf Edge	0.47 ± 0.10	0.56 ± 0.42	0.62 ± 0.30	0.41 ± 0.12
	CCS	1.31 ± 0.38	0.36 ± 0.25	0.75 ± 0.29	0.51 ± 0.29
	Site A	1.74 ± 0.36	1.69 ± 1.11	0.70 ± 0.18	1.39 ± 0.14
Fluorescence Index (FI)	Shelf Edge	1.25 ± 0.04	1.23 ± 0.37	1.08 ± 0.07	1.28 ± 0.05
	CCS	1.22 ± 0.08	1.19 ± 0.39	1.03 ± 0.07	1.30 ± 0.05
	Site A	1.30 ± 0.03	0.96 ± 0.02	0.83 ± 0.27	1.33 ± 0.05
Biological Index (BIX)	Shelf Edge	1.05 ± 0.04	1.24 ± 0.05	1.24 ± 0.05	0.99 ± 0.04
	CCS	0.98 ± 0.16	1.27 ± 0.04	1.26 ± 0.04	1.03 ± 0.05
	Site A	1.02 ± 0.06	1.28 ± 0.03	1.25 ± 0.02	0.97 ± 0.01
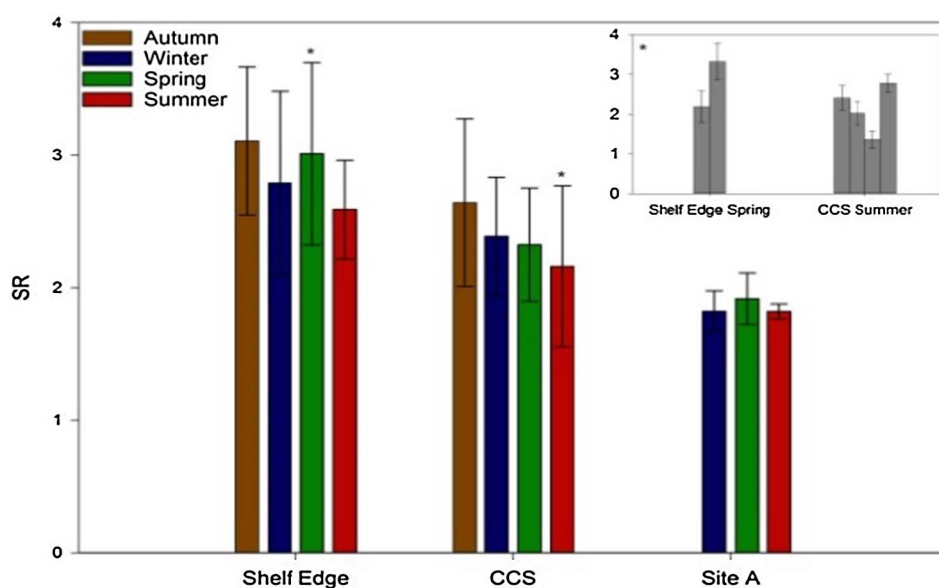
Fig. 7. Seasonal and cross shelf distribution of spectral slope ratio (SR). Bar plots represent the average water column SR for all data. Whiskers are one standard deviation of the average, thus an indication of temporal and water column variability. Autumn (brown bar), winter (blue bar), spring (green bar) and summer (red bar). *Insert bar charts for show individual vertical profile averages of water column SR for repeat station visits in instances were significant variability between visits and within seasons were identified (p < 0.05). (For interpretation of the references to colour in this figure legend, the reader is referred to the web version of this article.)

gradient in SR. In contrast, a305 and SUVA$_{280}$ were higher at Site A compared to the shelf edge (by 51% and 49%, respectively, p < 0.05), thus reversing the cross shelf gradient in comparison to the SR (Table 3).

Although the spectral slope $S_{300-650}$ values varied significantly between season (see above), the difference in the $S_{300-650}$ values were only significant in spring between Site A and CCS making it a poor descriptor of DOM composition over the spatial scales in this study.

The absolute values and range in HIX (0.11 and 3.64), FI (0.23 and 2.96) and BIX (0.71 and 1.39) are small in this study in comparison to the complete range that can occur in the natural environment. In isolation, they are of limited value in interpreting the source and dynamics of DOM but in combination with other environmental and optical data, they support our findings of strong cross shelf gradients in humic DOM but a strong seasonal trend in biologically associated DOM. At site A and CCS, HIX was highest in autumn (Table 3 and Supplementary Table 1), indicating DOM was more degraded and humified in autumn

compared to the rest of the year. HIX was lowest in spring at Site A and lowest in winter at CCS, suggesting DOM was fresher and less humified then. At the shelf edge, HIX was significantly lower in summer than spring (Supplementary Table 1). FI was significantly higher at all sites in summer than in spring (Supplementary Table 2). The range in averaged BIX was low (0.31 ± 0.16) and generally > 1 at all sites except Site A and the shelf edge in summer, and at CCS in autumn. BIX values were in the reported range for DOM of both autochthonous and bacterial origin.

The HIX was significantly higher at Site A than at the shelf edge throughout the year apart from spring when differences were not significant (Supplementary Table 2). Cross shelf gradients in FI and BIX were less clear and varied seasonally. Results from absorbance and fluorescence indices indicate a gradient in CDOM concentrations and composition persistent on seasonal time scales. High a305 coupled with high SUVA$_{280}$ and higher HIX values suggest that at Site A, there were greater concentrations of CDOM and that this material was higher

Table 4

Results of linear regression analysis between parameters in each season. Regression coefficients, intercept ± standard error (S.E.) and slope ± standard error (S.E.) are significant to $p < 0.05$. * Instances when regression coefficients are not significant $p > 0.05$.

| Parameters	Seasons	Intercept ± S.E.	Slope ± S.E.	R^2	Sample size
Salinity vs. C1	Autumn	0.87 ± 0.12	−0.024 ± 0.003	0.64	31
	Winter	1.13 ± 0.08	−0.031 ± 0.002	0.80	46
	Spring	0.75 ± 0.06	−0.021 ± 0.002	0.68	63
	Summer	0.61 ± 0.09	−0.017 ± 0.002	0.56	41
Salinity vs. C2	Autumn	0.64 ± 0.13	−0.018 ± 0.004	0.44	31
	Winter	0.75 ± 0.06	−0.021 ± 0.002	0.80	46
	Spring	0.64 ± 0.06	−0.018 ± 0.002	0.66	63
	Summer	0.62 ± 0.09	−0.017 ± 0.003	0.54	41
Salinity vs. C4	Autumn	0.68 ± 0.30	−0.019 ± 0.008	0.15	30
	Summer	0.47 ± 0.10	−0.013 ± 0.003	0.36	41
Salinity vs. DOC	Winter	1481 ± 252	−40 ± 7	0.48	36
	Summer	−642 ± 286	20 ± 8	0.13	45
Salinity vs. SR	Autumn	−129.5 ± 38.1	3.73 ± 1.1	0.23	42
	Winter	−72.0 ± 15.2	2.1 ± 0.4	0.36	45
	Spring	−76.0 ± 15.3	2.2 ± 0.4	0.37	47
	Summer	−43.6 ± 18.2	1.29 ± 0.5	0.14	40
Salinity vs. HIX	Autumn	118.7 ± 22.5	−3.32 ± 0.6	0.51	28
	Winter	100.3 ± 24.1	−2.82 ± 0.7	0.28	46
	Summer	50.4 ± 11.2	−1.41 ± 0.3	0.34	41
Salinity vs. SUVA$_{280}$	Autumn	21.49 ± 7.7	−0.60 ± 0.2	0.40	13
	Winter	10.53 ± 2.9	−0.28 ± 0.08	0.26	36
	Summer	24.50 ± 3.1	−0.68 ± 0.09	0.62	40
Salinity vs. a305	Winter	24.5 ± 2.6	−0.68 ± 0.07	0.67	46
	Summer	21.6 ± 2.8	−0.60 ± 0.08	0.61	40
C1 vs. DOC	Winter	46 ± 4	1347 ± 178	0.63	36
C1 vs. SR	Winter	3.3 ± 0.2	−56.0 ± 12.4	0.32	45
	Spring	3.6 ± 0.2	−83.3 ± 16.9	0.36	45
C1 vs. FI	Spring	1.22 ± 0.04	−14.95 ± 3.08	0.30	58
C1 vs. HIX	Autumn	0.09 ± 0.27*	97.6 ± 22.16	0.44	27
	Winter	−0.48 ± 0.38*	67.551 ± 20.44	0.20	46
	Summer	−0.28 ± 0.12	83.459 ± 10.72	0.61	41
C1 vs. a305	Winter	0.11 ± 0.03	20.429 ± 1.83	0.74	46
	Spring	0.20 ± 0.08	19.508 ± 5.19	0.20	59
	Summer	0.15 ± 0.03	30.725 ± 2.58	0.79	40
C1 vs. SUVA$_{280}$	Winter	0.39 ± 0.05	7.301 ± 2.53	0.20	36
	Spring	0.20 ± 0.10*	22.232 ± 6.60	0.25	36
	Summer	0.28 ± 0.05	26.289 ± 4.65	0.46	40
C2 vs. DOC	Winter	48 ± 4	1914 ± 291	0.56	36
C2 vs. SR	Winter	3.34 ± 0.24	−84.25 ± 18.66	0.32	45
	Spring	3.30 ± 0.23	−76.33 ± 20.77	0.24	45
C2 vs. HIX	Autumn	−0.03 ± 0.34*	109.76 ± 27.77	0.39	27
	Winter	−0.64 ± 0.37*	115.52 ± 29.5	0.26	46
	Summer	−0.24 ± 0.12	81.46 ± 10.47	0.61	41
C2 vs. SUVA$_{280}$	Autumn	0.74 ± 0.09	−31.92 ± 9.34	0.70	7
	Winter	0.38 ± 0.05	11.68 ± 3.75	0.22	36
	Summer	0.29 ± 0.05	25.43 ± 4.70	0.44	40
C2 vs. a305	Winter	0.12 ± 0.04	30.16 ± 2.86	0.72	46
	Summer	0.19 ± 0.04	27.21 ± 3.38	0.63	40
C4 vs. DOC	Autumn	33 ± 14	2649 ± 969	0.40	13
C4 vs. BIX	Autumn	0.86 ± 0.04	12.97 ± 3.01	0.40	30
C4 vs. FI	Winter	0.87 ± 0.02	16.17 ± 0.83	0.90	46
C4 vs. a305	Spring	0.29 ± 0.05	8.35 ± 2.34	0.20	53
	Summer	0.05 ± 0.07	25.47 ± 4.05	0.51	40
C4 vs. SUVA$_{280}$	Summer	0.18 ± 0.09*	23.01 ± 5.33	0.33	40
DOC vs. SR	Winter	3.95 ± 0.64	−0.02 ± 0.01	0.18	35
	Spring	−0.15 ± 1.04	0.04 ± 0.02	0.27	22
	Summer	0.75 ± 0.61	0.02 ± 0.01	0.13	40
DOC vs. $S_{300-650}$	Autumn	485 ± 7	1642 ± 640	0.29	18
DOC vs. a305	Winter	51 ± 5	42 ± 10	0.37	36
DOC vs. SUVA$_{280}$	Spring	80 ± 3	−24 ± 70	0.48	30
	Summer	88 ± 5	−38 ± 9	0.32	40
SR vs. SUVA$_{280}$	Spring	1.06 ± 0.13	−0.18 ± 0.05	0.32	28
SR vs. $S_{300-650}$	Summer	0.029 ± 0.001	−0.005 ± 0.001	0.68	40
HIX vs. a305	Summer	0.37 ± 0.03	0.17 ± 0.05	0.26	40
FI vs. SUVA$_{280}$	Autumn	1.74 ± 0.38	−1.16 ± 0.33	0.67	8
	Spring	1.29 ± 0.24	−0.79 ± 0.24	0.27	32
a305 vs. $S_{300-650}$	Autumn	0.02 ± 0.002	−0.02 ± 0.004	0.38	42
a305 vs. SUVA$_{280}$	Autumn	0.07 ± 0.06*	0.80 ± 0.12	0.80	13
	Winter	0.29 ± 0.04	0.49 ± 0.08	0.52	36
	Spring	0.04 ± 0.09*	0.93 ± 0.16	0.48	39
	Summer	0.13 ± 0.05	0.91 ± 0.11	0.65	40

N. Carr et al.
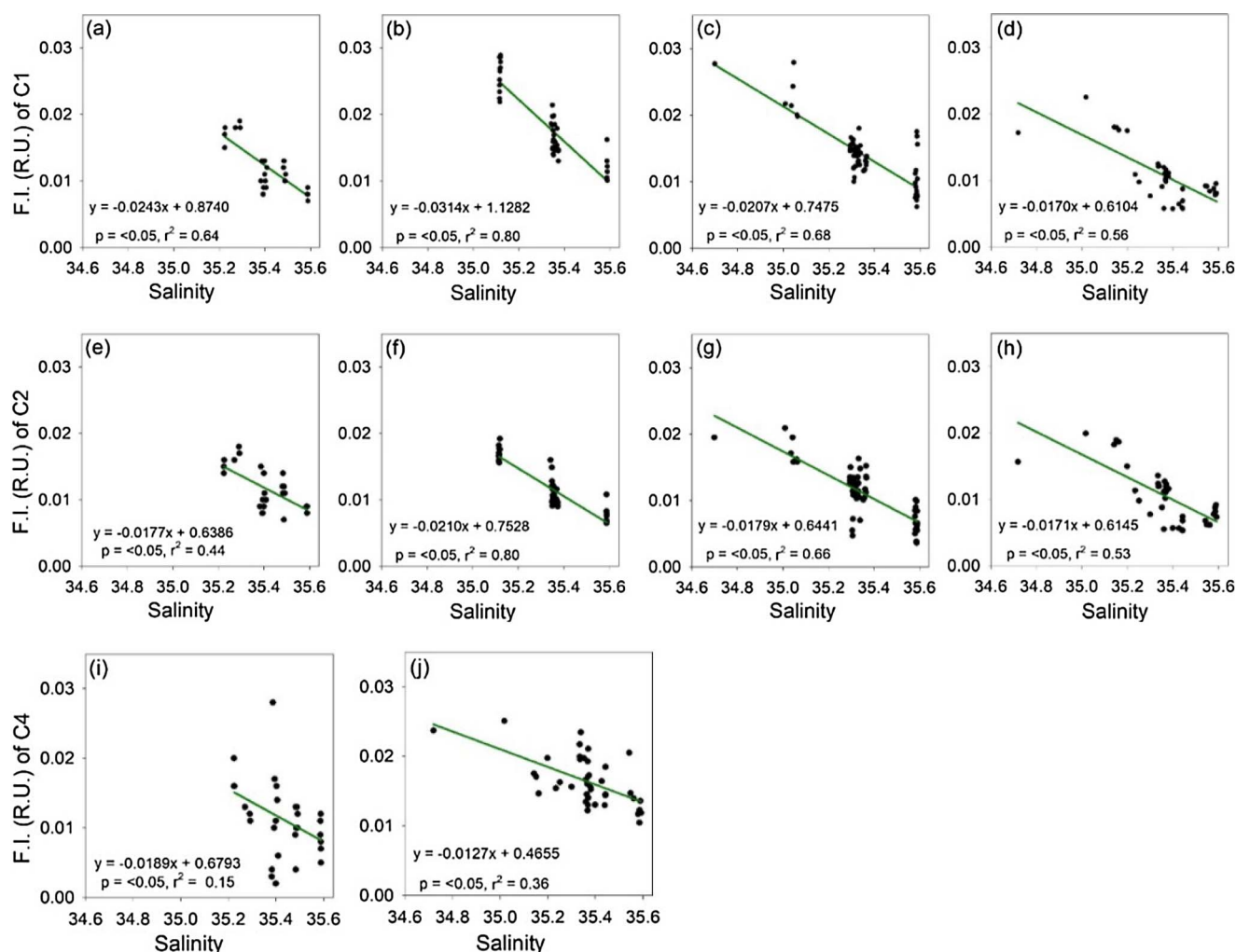
Fig. 8. Relationships of salinity with fluorescence intensity of PARAFAC components; C1 for autumn (a), winter (b), spring (c) and summer (d); C2 for autumn (e), winter (f), spring (g) and summer (h); and with C4 for autumn (i) and summer (j).

molecular weight and more aromatic than compared to the shelf edge site, characterised by DOM of lower molecular weight.

3.4. Relationships between DOC, DOM components, CDOM spectral indices and salinity

The relationship between parameters was determined by linear regression analysis (Table 4). DOC and salinity were negatively correlated in winter and weakly positively correlated in summer. Fluorescence intensity of components C1 and C2 were negatively correlated with salinity throughout the year, the relationships varied seasonally, with the strongest relationships being observed in winter ($r^2 = 0.80$) (Fig. 8a–d and e–f, respectively). The C4 component was weakly negatively correlated with salinity during autumn and summer and similarly to C1 and C2, the relationship varied between seasons (Fig. 8i–j). C3 was not correlated with salinity. The SR was weakly positively correlated with salinity, the relationship varied seasonally and was strongest in spring ($r^2 = 0.37$), and weakest in summer ($r^2 = 0.14$). HIX and SUVA$_{280}$ were negatively correlated with salinity except in spring, and a305 was negatively correlated with salinity in winter and summer. Although the salinity range sampled across the shelf sea throughout the different seasons was low (< 1), consistent and significant relationships with C1 and C2 indicate the presence of the terrestrially derived end-member.

There were strong positive correlations between DOC and C1 and C2 during winter ($r^2 = 0.63$ and 0.56, respectively) (Fig. 9b and c,

respectively). DOC was also positively correlated with C4 (Fig. 9a) and $S_{300-650}$ during autumn, with a305 in winter and negatively correlated with SUVA$_{280}$ in spring and summer (Table 4). The relationship between DOC and the SR reversed from negative in winter to positive during spring and summer, with the relationship being strongest in spring ($r^2 = 0.27$).

DOM components C1, C2 and C4 were correlated to spectral indices to varying strengths and during different seasons (Table 4). C1 and C2 were negatively correlated with the SR in winter and spring, positive correlations with the HIX in autumn, winter and summer when the relationships were strongest ($r^2 = 0.61$), and with SUVA$_{280}$ and a305 in winter and summer. C4 was positively correlated with SUVA$_{280}$ in summer, a305 in spring and summer, with the BIX in autumn and with FI in winter ($r^2 = 0.90$).

4. Discussion

4.1. Factors driving seasonality in DOC

There was no consistent seasonal trend in DOC at stations sampled in the Celtic Sea. Instead, seasonality was site specific and it is likely that the physical and biogeochemical characteristics at each site were a strong determinant for the patterns observed.

High DOC observed at Site A in autumn is likely due to local production and external inputs. High C3 and BIX values indicate a predominantly biological and bacterial source of DOM, implying the
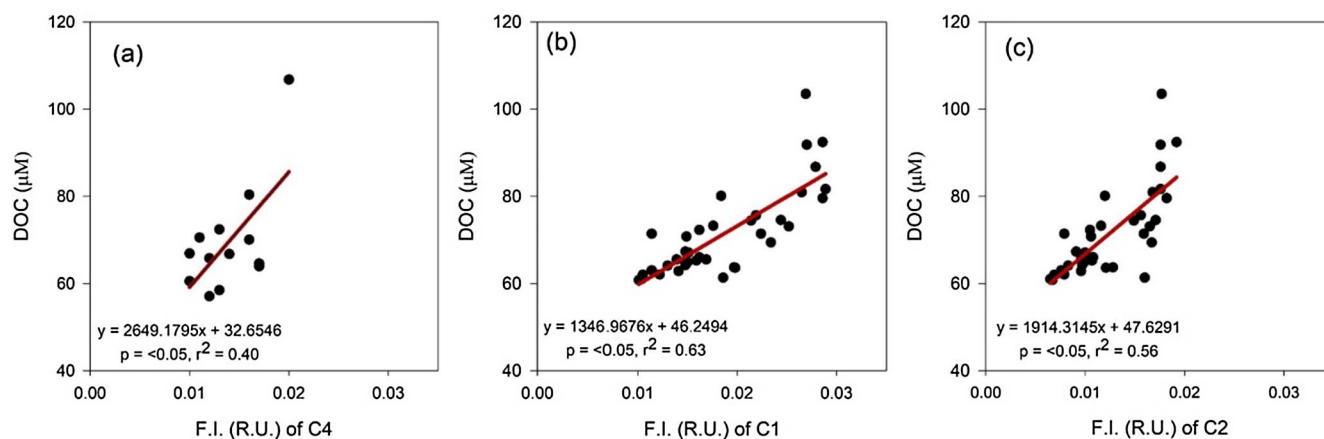
Fig. 9. Distribution of DOC as a function of fluorescence intensity of fluorescence components (a) C4 in autumn, (b) C1 in winter and (c) C2 in winter.

autumn bloom and/or remineralisation of POM was a source of DOC. In addition, FI values of 1.3 and high HIX values alongside negative correlations between salinity and humic-like DOM and C4 suggests an external terrestrial input which could account for high DOC concentrations at Site A in autumn. DOC was lowest in summer at Site A. This was likely a result of a reduction in DOC production by 1.4-fold compared to the preceding spring (Garcia-Martin et al., this issue, Poulton et al., this issue) as well as reduced discharge and DOC input from the River Severn between winter ($242 \, m^3 \, s^{-1}$ and $7699 \, \mu M$ $DOC \, d^{-1}$ respectively in January 2015) and spring ($96 \, m^3 \, s^{-1}$ and $2559 \, \mu M \, DOC \, d^{-1}$, respectively in March 2015) (Leeuwen, 2017).

At CCS, high DOC concentrations in spring coincided with the highest DOC production rates (Garcia-Martin et al., this issue). Low DOC in summer coincided with the highest bacterial production and lowest bacterial respiration observed at CCS, implying net consumption of DOC by bacteria at this site (Garcia-Martin et al., this issue). Higher DOC at the shelf edge site in summer probably reflects net production of DOC during sustained productivity following the spring bloom. Lower DOC in winter may reflect the influence of deep or open ocean waters onto the shelf (as noted by (Humphreys et al., this issue, Ruiz-Castillo et al., this issue), which have lower DOC concentrations relative to shelf waters.

DOC production in autumn, spring and summer at CCS and the shelf edge was greater than bacterial carbon demand (BCD) (Garcia-Martin et al., this issue), and at CCS DOC:DON ranged from 12.4 ± 0.2 in summer to a maximum of 17.0 ± 3.4 in spring (Davis et al., this issue), greater than the Redfield ratio of 6.6:1 (Redfield, 1934). However, (Poulton et al., this issue) found that C-overconsumption by phytoplankton was not dominant in the Celtic Sea but instead other biogeochemical processes driven by bacteria and/or zooplankton are likely to create more C-rich material which would contribute to the continental shelf pump. Thus, there is accumulating evidence for the importance of DOM as a vehicle for export of carbon from the shelf sea.

4.2. Input of terrestrial OM in the shelf sea

There were strong cross shelf gradients in C1 during all seasons in the Celtic Sea, being consistently higher at Site A and lower at the shelf edge, reflecting input of a terrestrial humic component in the nearshore environment and dilution across the shelf (Murphy et al., 2008, Kowalczuk et al., 2013). Seasonal variation in the inverse relationship between C1 and salinity likely reflects seasonality in inputs (Leeuwen, 2017) alongside seasonal changes in physical transport and hydrography (Ruiz-Castillo et al., this issue). Terrestrial humic material is susceptible to photo-degradation and up to 96% of CDOM and 41% of DOC from freshwater sources can be destroyed by solar radiation in the

surface mixed layer (Vahatalo and Wetzel, 2004). C1 was generally lower in the surface, however, no distinct vertical gradients were observed in this study.

DOC and salinity were negatively correlated in autumn (not significant) and winter ($r^2 = 0.48$, $p < 0.05$) and positively correlated in spring (not significant) and summer ($r^2 = 0.13$, $p < 0.05$). Reversal of the cross shelf gradients and change in slope reflects seasonality in inputs (see Section 4.1), seasonality in transport (Ruiz-Castillo et al., this issue) and biological production and consumption (Garcia-Martin et al., this issue, Poulton et al., this issue).

Cross shelf gradients in the slope ratio (SR) provides further evidence for the influence of terrestrially-derived DOM in the Celtic sea. The slope ratio (SR) has been shown to be inversely related to CDOM molecular weight (MW) (Helms et al., 2008). The persistent weak positive correlation between SR and salinity implies input of terrestrially-derived higher MW DOM at the freshwater end member in contrast to a fresher low MW or photo-degraded DOM pool at the shelf edge (Stubbins et al., 2012). Correlations between SR and DOC were weak but changed from negative in winter to positive in summer, when DOC and $SUVA_{280}$ were also negatively correlated. Indeed, consistently higher values for a305, $SUVA_{280}$ and HIX at Site A compared to the rest of the Celtic Sea again provides further evidence for input of terrestrially-derived high MW DOM into the northern Celtic Sea, especially in winter.

In winter, DOC was strongly correlated with C1, when 62% of the DOC distribution was explained by C1 and an intercept value of 46 ± 3 μM indicated that a substantial fraction of DOC (potentially up to 45%) was non-absorbing (Mendoza and Zika, 2014). However, when employing the salinity DOC winter regression coefficients, there was a large freshwater end member for DOC (1481 ± 252 μM) of which potentially 815 ± 139 μM of DOC was absorbing. This freshwater end member was over three times greater than the average freshwater end member, 465 ± 12 μM of Barron and Duarte (2015) but within the total range reported for freshwater DOC end members (0–2500 μM). Using the slope and intercept values of the relationship between salinity, DOC and C1 (Table 4), we estimate that a maximum of 25 μM of DOC was of terrestrial origin at CCS in winter, representing 35% of the DOC pool (CCS average salinity of 35.35), being 43% at Site A and 24% at the shelf edge. This estimate is high considering that riverine nitrate and nitrite (N + N) only accounts for up to 10% of total N + N at the CCS site (Ruiz-Castillo et al., this issue) and that CCS is 200 km for the nearest coast and 400 km from the Bristol Channel. The contribution of terrestrially-derived DOM to the open ocean has not been fully quantified, however new insights into the mechanisms for its transport, transformation and fate are emerging (Lauerwald et al., 2012, Raymond and Spencer, 2015, Osburn et al., 2016).

4.3. Biological production of OM in the shelf sea

There were strong temporal variations in the protein-like components, C3 and C4 linked to productive periods. For example, C4 increased by 91% from autumn to spring at CCS. Even on shorter timescales of hours to days, when net primary production (NPP) increased 3-fold over a period of four days at CCS (from 154 mmol C m^{-2} d^{-1} to 532.1 mmol C m^{-2} d^{-1}, (Poulton et al., this issue)), C3 and C4 increased rapidly. Despite the strong link to biological production, no correlation between C3 or C4 and chlorophyll *a* was observed, possibly due to the patchiness in biological activity as observed in measurements of NPP (Poulton et al., this issue) and gross oxygen production (Seguro et al., this issue). These protein-like components are considered to represent the bioavailable fraction of the DOM pool (Yamashita and Tanoue, 2003, Jaffe et al., 2014), and are commonly attributed to autochthonous in situ production by bacterial and phytoplankton (Vantrepotte et al., 2007, Murphy et al., 2008, Mendoza and Zika, 2014, Danhiez et al., 2017). Such rapid changes in these components have been observed previous, for example, in the Arctic Ocean following a phytoplankton bloom (Chen et al., 2017) and in the Florida Everglades (Chen and Jaffe, 2014).

Winter maxima were observed in the protein-like components, specifically C3 at Site A and CCS and C4 at the shelf edge. The reason for the occurrence of labile DOM in winter in the Celtic Sea is currently unclear but may be due to remineralisation of POM to dissolved labile compounds over the winter period, or the occurrence of stochastic winter blooms, as observed in the subpolar North Atlantic (Lacour et al., 2017) resulting in release of fresh DOM prior to the spring bloom.

Similarly to other studies (Jorgensen et al., 2011, Kowalczuk et al., 2013, Mendoza and Zika, 2014), there was no significant correlation between C3 and salinity, suggesting that the cross shelf distribution of C3 was driven mainly by non-conservative mixing and in situ production. In contrast, C4 was correlated with salinity, as observed elsewhere (Mendoza and Zika, 2014, Pitta et al., 2016), and at times followed a terrestrial type distribution (Murphy et al., 2008). C4 also correlated with SUVA$_{280}$, a305, BIX and FI suggest that C4 was produced from substrates of both terrestrial and autochthonous origin.

The increase in a305 and SUVA$_{280}$ from winter to spring to summer indicates that there is an increase in the aromaticity of the DOM, which implies an increase in MW or refractory component of DOM. Rather than being indicative of a terrestrial source, we postulate that in situ bacterial processing of the DOM pool is likely to have increased the aromaticity of the DOM (Cuss and Gueguen, 2015, Hansen et al., 2016), at Site A from winter to summer. This observation highlights the complexity in the DOM pool as both supply and in situ processing operate simultaneously.

5. Conclusions

This study demonstrated the strength of a multi-dimensional approach incorporating DOM optical properties alongside measurements of DOC in delineating the complexities of the DOM pool in shelf seas.

Seasonality in DOC concentrations was site specific reflecting contrasting physical and biological conditions at each site. Strong cross shelf gradients in C1, C2, SR, a305, SUVA$_{280}$ and HIX, as well as strong correlations between salinity and DOC, C1, HIX, SUVA$_{280}$ and a305 indicate the input and influence of terrestrially-derived DOM to the DOC pool in the Celtic Sea. Using these correlations, we estimate that terrestrial DOM represented 24, 35 and 43% of the total DOC pool at the shelf edge, CCS and Site A, respectively. Significant temporal variation in C3 and C4, also highlighted the importance of biological production and consumption in influencing DOC concentrations in the Celtic Sea over short (hours to days) and longer (seasonal) timescales.

Site A was strongly influenced by inputs from land and the DOM pool reflected this due to the dominance of high MW and humified DOM. In contrast, the shelf edge was characterised by low MW and

fresher DOM. Overall, there is accumulating evidence from this study and other studies on bacterial carbon dynamics (Garcia-Martin et al., this issue), phytoplankton carbon dynamics (Poulton et al., this issue) and the stoichiometry of DOM and POM (Davis et al., this issue), highlighting the potential importance of the DOM pool as a vehicle for transport of C from the shelf. This study contributes to this emerging idea by providing insight into the seasonality and composition of the DOM pool, thus identifying when the DOM pool is likely to be most efficient at exporting carbon. Further examination is needed on how bacteria and phytoplankton interact with the different DOM pools, both refractory and labile, over the timescales relevant for carbon export from shelf seas. This will help determine the relative magnitude of on shelf processing versus off shelf export of DOM.

Appendix A. Supplementary material

Supplementary data associated with this article can be found, in the online version, at http://dx.doi.org/10.1016/j.pocean.2018.02.025.

References

Aluwihare, L.I., Repeta, D.J., Chen, R.F., 2002. Chemical composition and cycling of dissolved organic matter in the Mid-Atlantic Bight. Deep-Sea Res. Part Ii-Topical Stud. Oceanogr. 49 (20), 4421–4437.

Andersson, C.A., Bro, R., 2000. The N-way toolbox for MATLAB. Chemometr. Intelligent Laboratory Syst. 52 (1), 1–4.

Bai, Y., Rongguo, S., Qingzhen, Y., Zhang, C., Shi, X., 2017. Characterization of Chromophoric Dissolved Organic Matter (CDOM) in the Bohai Sea and the Yellow Sea Using Excitation-Emission Matrix Spectroscopy (EEMs) and Parallel Factor Analysis (PARAFAC). Estuaries Coasts.

Barron, C., Duarte, C.M., 2015. Dissolved organic carbon pools and export from the coastal ocean. Global Biogeochem. Cycles 29 (10), 1725–1738.

Bro, R., 1997. PARAFAC. Tutorial and applications. Chemometr. Intelligent Laboratory Syst. 38 (2), 149–171.

Cai, W.J., 2011. Estuarine and Coastal Ocean Carbon Paradox: CO2 Sinks or Sites of Terrestrial Carbon Incineration? Ann. Rev. Mar. Sci., Vol 3. C. A. Carlson and S. J. Giovannoni. 3, pp. 123–145.

Catala, T.S., Reche, I., Alvarez, M., Khatiwala, S., Guallart, E.F., Benitez-Barrios, V.M., Fuentes-Lema, A., Romera-Castillo, C., Nieto-Cid, M., Pelejero, C., Fraile-Nuez, E., Ortega-Retuerta, E., Marrase, C., Alvarez-Salgado, X.A., 2015. Water mass age and aging driving chromophoric dissolved organic matter in the dark global ocean. Global Biogeochem. Cycles 29 (7), 917–934.

Chen, M., Nam, S.-I., Kim, J.-H., Kwon, Y.-J., Hong, S., Jung, J., Shin, K.-H., Hur, J., 2017. High abundance of protein-like fluorescence in the Amerasian Basin of Arctic Ocean: Potential implication of a fall phytoplankton bloom. Sci. Total Environ. 599–600, 355–363.

Chen, M.L., Jaffe, R., 2014. Photo- and bio-reactivity patterns of dissolved organic matter from biomass and soil leachates and surface waters in a subtropical wetland. Water Res. 61, 181–190.

Coble, P.G., 1996. Characterization of marine and terrestrial DOM in seawater using excitation emission matrix spectroscopy. Mar. Chem. 51 (4), 325–346.

Cuss, C.W., Gueguen, C., 2015. Relationships between molecular weight and fluorescence properties for size-fractionated dissolved organic matter from fresh and aged sources. Water Res. 68, 487–497.

D'Sa, E.J., Steward, R.G., Vodacek, A., Blough, N.V., Phinney, D., 1999. Determining optical absorption of colored dissolved organic matter in seawater with a liquid capillary waveguide. Limnol. Oceanogr. 44 (4), 1142–1148.

Danhiez, F.P., Vantrepotte, V., Cauvin, A., Lebourg, E., Loisel, H., 2017. Optical properties of chromophoric dissolved organic matter during a phytoplankton bloom. Implication for DOC estimates from CDOM absorption. Limnol. Oceanogr. 62 (2).

Davis, C.E., Blackbird, S., Wolff, G., Woodward, E.M.S., Mahaffey, C., this issue. Seasonal organic matter dynamics in a temperate shelf sea. Progress in Oceanography this issue.

Eglinton, T.I., Repeta, D.J., 2006. Organic Matter in the Contemporary Ocean in: The Oceans and Marine Geochemistry Elsevier.

García-Martín, E.E., Daniels, C.J., Davidson, K., Lozano, J., Mayers, K.M.J., McNeil,S.,

Mitchell, E., Poulton, A.J., Purdie, D.A., Tarran, G.A., Whyte, C., Robinson, C., this issue. Seasonal changes in plankton respiration and bacterial metabolism in a temperate Shelf Sea. Progress in Oceanography, this issue.

Green, S.A., Blough, N.V., 1994. Optical absorption and fluorescence properties of chromophoric dissolved organic matter in natural waters. Limnol. Oceanogr. 39 (8), 1903–1916.

Hansell, D.A., 2013. Recalcitrant dissolved organic carbon fractions. Ann. Rev. Mar. Sci., Vol 5. C A. Carlson and S J. Giovannoni. 5, 421–445.

Hansell, D.A., Carlson, C.A., 1998. Deep-ocean gradients in the concentration of dissolved organic carbon. Nature 395 (6699), 263–266.

Hansell, D.A., Carlson, C.A., 2001. Marine dissolved organic matter and the carbon cycle. Oceanography 14.

Hansell, D.A., Carlson, C.A., 2015. DOM sources, sinks, reactivity, and budgets. In: Hansell, D.A., Carlson, C.A. (Eds.), Biogeochemistry of Marine Dissolved Organic Matter. Academic Press, London, pp. 65–126.

Hansell, D.A., Carlson, C.A., Repeta, D.J., Schlitzer, R., 2009. Dissolved Organic Matter in the ocean A controversy stimulates new insights. Oceanography 22 (4), 202–211.

Hansen, A.M., Kraus, T.E.C., Pellerin, B.A., Fleck, J.A., Downing, B.D., Bergamaschi, B.A., 2016. Optical properties of dissolved organic matter (DOM): Effects of biological and photolytic degradation. Limnol. Oceanogr. 61 (3), 1015–1032.

Hedges, J.I., Keil, R.G., Benner, R., 1997. What happens to terrestrial organic matter in the ocean? Org. Geochem. 27 (5–6), 195–212.

Helms, J.R., Stubbins, A., Ritchie, J.D., Minor, E.C., Kieber, D.J., Mopper, K., 2008. Absorption spectral slopes and slope ratios as indicators of molecular weight, source, and photobleaching of chromophoric dissolved organic matter. Limnol. Oceanogr. 53 (3), 955–969.

Hopkinson, C.S., Vallino, J.J., 2005. Efficient export of carbon to the deep ocean through dissolved organic matter. Nature 433 (7022), 142–145.

Huguet, A., Vacher, L., Relexans, S., Saubusse, S., Froidefond, J.M., Parlanti, E., 2009. Properties of fluorescent dissolved organic matter in the Gironde Estuary. Org. Geochem. 40 (6), 706–719.

Humphreys, M.P., Achterberg, E.P., Chowdhury, M.Z.H., Griffiths, A.M., Hartman, S., Hopkins, J.E., Hull, T., Kivimäe, C., Smilenova, A., Wihsgott, J., Woodward, E.M.S., Moore, C.M., this issue. Mechanisms for a nutrient-conserving carbon pump in a seasonally stratified, temperate continental shelf sea. Progress in Oceanography this issue.

Hygum, B.H., Petersen, J.W., Sondergaard, M., 1997. Dissolved organic carbon released by zooplankton grazing activity - A high-quality substrate pool for bacteria. J. Plankton Res. 19 (1), 97–111.

Jaffe, R., Cawley, K.M., Yamashita, Y., 2014. Applications of Excitation Emission Matrix Fluorescence with Parallel Factor Analysis (EEM-PARAFAC) in Assessing Environmental Dynamics of Natural Dissolved Organic Matter (DOM) in Aquatic Environments: A Review. Advances in the Physicochemical Characterization of Dissolved Organic Matter: Impact on Natural and Engineered Systems. F. RosarioOrtiz. 1160: 27-+.

Jiao, N., Herndl, G.J., Hansell, D.A., Benner, R., Kattner, G., Wilhelm, S.W., Kirchman, D.L., Weinbauer, M.G., Luo, T.W., Chen, F., Azam, F., 2010. Microbial production of recalcitrant dissolved organic matter: long-term carbon storage in the global ocean. Nat. Rev. Microbiol. 8 (8), 593–599.

Jorgensen, L., Stedmon, C.A., Kragh, T., Markager, S., Middelboe, M., Sondergaard, M., 2011. Global trends in the fluorescence characteristics and distribution of marine dissolved organic matter. Mar. Chem. 126 (1–4), 139–148.

Kowalczuk, P., Tilstone, G.H., Zablocka, M., Rottgers, R., Thomas, R., 2013. Composition of dissolved organic matter along an Atlantic Meridional Transect from fluorescence spectroscopy and Parallel Factor Analysis. Mar. Chem. 157, 170–184.

Lacour, L., Ardyna, M., Stec, K.F., Claustre, H., Prieur, L., Poteau, A., D'Alcala, M.R., Iudicone, D., 2017. Unexpected winter phytoplankton blooms in the North Atlantic subpolar gyre. Nat. Geosci. 10 (11), 836–839.

Lauerwald, R., Hartmann, J., Ludwig, W., Moosdorf, N., 2012. Assessing the non-conservative fluvial fluxes of dissolved organic carbon in North America. J. Geophys. Res.-Biogeosci. 117.

Leeuwen, S.M., 2017. UK data was processed from raw data provided by the Environment Agency, the Scottish Environment Protection Agency, the Rivers Agency (Northern Ireland) and the National River Flow Archive. Dr. S.M. van Leeuwen, CEFAS, Lowestoft, UK, pers. comm.

Liu, K.K., Atkinson, L., Quinones, R.A., Talaue-McManus, L., 2010. Biogeochemistry of Continental Margins in a Global Context. Carbon and Nutrient Fluxes in Continental Margins: A Global Synthesis. K.K. Liu, L. Atkinson, R. Quinones and L. TalaueMcManus, pp. 3–24.

Lu, Y.H., Edmonds, J.W., Yamashita, Y., Zhou, B., Jaegge, A., Baxley, M., 2015. Spatial variation in the origin and reactivity of dissolved organic matter in Oregon-Washington coastal waters. Ocean Dyn. 65 (1), 17–32.

Mayers, K.M.J., Poulton, A.J., Daniels, C.J., Wells, S.R., Woodward, E.M.S., Tarran, G.A., Widdicombe, C.E., Mayor, D.J., Atkinson, A., Giering, S.L.C., this issue. Top-down control of coccolithophore populations during spring in a temperate Shelf 616 Sea (Celtic Sea, April 2015). Progress in Oceanography.

McKnight, D.M., Boyer, E.W., Westerhoff, P.K., Doran, P.T., Kulbe, T., Andersen, D.T., 2001. Spectrofluorometric characterization of dissolved organic matter for indication of precursor organic material and aromaticity. Limnol. Oceanogr. 46 (1), 38–48.

Mendoza, W.G., Zika, R.G., 2014. On the temporal variation of DOM fluorescence on the southwest Florida continental shelf. Prog. Oceanogr. 120, 189–204.

Murphy, K.R., Stedmon, C.A., Graeber, D., Bro, R., 2013. Fluorescence spectroscopy and multi-way techniques. PARAFAC. Anal. Methods 5 (23), 6557–6566.

Murphy, K.R., Stedmon, C.A., Waite, T.D., Ruiz, G.M., 2008. Distinguishing between terrestrial and autochthonous organic matter sources in marine environments using fluorescence spectroscopy. Mar. Chem. 108 (1–2), 40–58.

Nelson, N.B., Siegel, D.A., 2013. The global distribution and dynamics of chromophoric dissolved organic matter. Ann. Rev. Mar. Sci., Vol 5. C A. Carlson and S. J. Giovannoni. 5, 447–476.

Ohno, T., 2002. Fluorescence inner-filtering correction for determining the humification index of dissolved organic matter. Environ. Sci. Technol. 36 (4), 742–746.

Osburn, C.L., Boyd, T.J., Montgomery, M.T., Bianchi, T.S., Coffin, R.B., Paerl, H.W., 2016. Optical proxies for terrestrial dissolved organic matter in estuaries and coastal waters. Front. Mar. Sci. 2 (127).

Pitta, E., Zeri, C., Tzortziou, M., Mousdis, G., Scoullos, M., 2016. Seasonal variations in dissolved organic matter composition using absorbance and fluorescence spectroscopy in the Dardanelles Straits – North Aegean Sea mixing zone. Cont. Shelf Res.

Poulton, A.J., Davis, C.E., Daniels, C.J., Mayers, K.M.J., Harris, C., Tarran, G.A., Widdicome, C.E., Woodward, E.M.S., this issue. Seasonal phosphorus and carbon dynamics in a temperate shelf sea (Celtic Sea). Progress in Oceanography, this issue.

Raymond, P.A., Spencer, R.G.M., 2015. Riverine DOM. In: Hansell, D.A., Carlson, C.A. (Eds.), Biogeochemistry of Marine Dissolved Organic Matter. Academic Press, London, pp. 509–533.

Redfield, A.C., 1934. On the proportions of organic derivatives in sea water and their relation to the composition of plankton. James Johnstone Memorial Volume, University Press of Liverpool, pp. 176–192.

Repeta, D.J., Quan, T.M., Aluwihare, L.I., Accardi, A.M., 2002. Chemical characterization of high molecular weight dissolved organic matter in fresh and marine waters. Geochimica Et Cosmochimica Acta 66 (6), 955–962.

Ruiz-Castillo, E., Sharples, J., Hopkins, J.E., Woodward, E.M.S., this issue. Seasonality in the cross-shelf physical structure of a temperate shelf sea and the implications for nutrient supply and carbon export. Progress in Oceanography, this issue.

Seguro, I., Marca, A.D., Painting, S.J., Shutler, J.D., Sugget, D.J., Kaiser, J., this issue. High-resolution net and gross biological production during a Celtic Sea spring bloom. Progress in Oceanography this issue.

Sipler, R.E., Bronk, D.A., 2015. Dynamics of dissolved organic nitrogen. In: Hansell, D.A., Carlson, C.A. (Eds.), Biogeochemistry of Marine Dissolved Organic Matter. Academic Press, London, pp. 127–232.

Stedmon, C.A., Amon, R.M.W., Rinehart, A.J., Walker, S.A., 2011. The supply and characteristics of colored dissolved organic matter (CDOM) in the Arctic Ocean: Pan Arctic trends and differences. Mar. Chem. 124 (1–4), 108–118.

Stedmon, C.A., Bro, R., 2008. Characterizing dissolved organic matter fluorescence with parallel factor analysis: a tutorial. Limnol. Oceanogr.-Methods 6, 572–579.

Stedmon, C.A., Markager, S., Bro, R., 2003. Tracing dissolved organic matter in aquatic environments using a new approach to fluorescence spectroscopy. Mar. Chem. 82 (3–4), 239–254.

Stedmon, C.A., Markager, S., Kaas, H., 2000. Optical properties and signatures of chromophoric dissolved organic matter (CDOM) in Danish coastal waters. Estuar. Coast. Shelf Sci. 51 (2), 267–278.

Stedmon, C.A., Nelson, N.B., 2015. The Optical Properties of DOM in the Ocean. In: Hansell, D.A., Carlson, C.A. (Eds.), Biogeochemistry of Marine Dissolved Organic Matter. Academic Press, London, pp. 481–508.

Stubbins, A., Lapierre, J.F., Berggren, M., Prairie, Y.T., Dittmar, T., del Giorgio, P.A., 2014. What's in an EEM? Molecular Signatures Associated with Dissolved Organic Fluorescence in Boreal Canada. Environ. Sci. Technol. 48 (18), 10598–10606.

Stubbins, A., Niggemann, J., Dittmar, T., 2012. Photo-lability of deep ocean dissolved black carbon. Biogeosciences 9 (5), 1661–1670.

Suttle, C.A., 2005. Viruses in the sea. Nature 437 (7057), 356–361.

Suttle, C.A., 2007. Marine viruses - major players in the global ecosystem. Nat. Rev. Microbiol. 5 (10), 801–812.

Vahatalo, A.V., Wetzel, R.G., 2004. Photochemical and microbial decomposition of chromophoric dissolved organic matter during long (months-years) exposures. Mar. Chem. 89 (1–4), 313–326.

Vantrepotte, V., Brunet, C., Meriaux, X., Lecuyer, E., Vellucci, V., Santer, R., 2007. Bio-optical properties of coastal waters in the Eastern English Channel. Estuar. Coast. Shelf Sci. 72 (1–2), 201–212.

Weishaar, J.L., Aiken, G.R., Bergamaschi, B.A., Fram, M.S., Fujii, R., Mopper, K., 2003. Evaluation of specific ultraviolet absorbance as an indicator of the chemical composition and reactivity of dissolved organic carbon. Environ. Sci. Technol. 37 (20), 4702–4708.

Yamashita, Y., Fichot, C.G., Shen, Y., Jaffé, R., Benner, R., 2015. Linkages among fluorescent dissolved organic matter, dissolved amino acids and lignin-derived phenols in a river-influenced ocean margin. Front. Mar. Sci. 2 (92).

Yamashita, Y., Panton, A., Mahaffey, C., Jaffe, R., 2011. Assessing the spatial and temporal variability of dissolved organic matter in Liverpool Bay using excitation-emission matrix fluorescence and parallel factor analysis. Ocean Dyn. 61 (5), 569–579.

Yamashita, Y., Tanoue, E., 2003. Chemical characterization of protein-like fluorophores in DOM in relation to aromatic amino acids. Mar. Chem. 82 (3–4), 255–271.

Zhao, Z., Gonsior, M., Luek, J., Timko, S., Ianiri, H., Hertkorn, N., Schmitt-Kopplin, P., Fang, X.T., Zeng, Q.L., Jiao, N.Z., Chen, F., 2017. Picocyanobacteria and deep-ocean fluorescent dissolved organic matter share similar optical properties. Nat. Commun. 8.

Zsolnay, A., Baigar, E., Jimenez, M., Steinweg, B., Saccomandi, F., 1999. Differentiating with fluorescence spectroscopy the sources of dissolved organic matter in soils subjected to drying. Chemosphere 38 (1), 45–50.